

# 1 **The formation and mitigation of nitrate pollution:**

## 2 **Comparison between urban and suburban environments**

3 Suxia Yang<sup>1,2</sup>, Bin Yuan<sup>1,2\*</sup>, Yuwen Peng<sup>1,2</sup>, Shan Huang<sup>1,2</sup>, Wei Chen<sup>3</sup>, Weiwei Hu<sup>3</sup>,  
4 Chenglei Pei<sup>3,4,5,6</sup>, Jun Zhou<sup>1,2</sup>, David D. Parrish<sup>1</sup>, Wenjie Wang<sup>7</sup>, Xianjun He<sup>1,2</sup>,  
5 Chunlei Cheng<sup>2,8</sup>, Xiaobing Li<sup>1,2</sup>, Xiaoyun Yang<sup>1,2</sup>, Yu Song<sup>7</sup>, Haichao Wang<sup>9</sup>, Jipeng  
6 Qi<sup>1,2</sup>, Baolin Wang<sup>10</sup>, Chen Wang<sup>10</sup>, Chaomin Wang<sup>1,2</sup>, Zelong Wang<sup>1,2</sup>, Tiange Li<sup>1,2</sup>,  
7 E Zheng<sup>1,2</sup>, Sihang Wang<sup>1,2</sup>, Caihong Wu<sup>1,2</sup>, Mingfu Cai<sup>1,2</sup>, Chenshuo Ye<sup>7</sup>, Wei Song<sup>3</sup>,  
8 Peng Cheng<sup>8</sup>, Duohong Chen<sup>6</sup>, Xinming Wang<sup>3</sup>, Zhanyi Zhang<sup>1,2</sup>, Xuemei Wang<sup>1,2</sup>,  
9 Junyu Zheng<sup>1,2</sup>, Min Shao<sup>1,2\*</sup>

10 <sup>1</sup>Institute for Environmental and Climate Research, Jinan University, Guangzhou  
11 511443, China

12 <sup>2</sup>Guangdong-Hongkong-Macau Joint Laboratory of Collaborative Innovation for  
13 Environmental Quality, Jinan University, Guangzhou 511443, China

14 <sup>3</sup>State Key Laboratory of Organic Geochemistry and Guangdong Key Laboratory of  
15 Environmental Protection and Resources Utilization, Guangzhou Institute of  
16 Geochemistry, Chinese Academy of Sciences, Guangzhou 510640, China

17 <sup>4</sup>CAS Center for Excellence in Deep Earth Science, Guangzhou, 510640, China

18 <sup>5</sup>University of Chinese Academy of Sciences, Beijing 100049, China

19 <sup>6</sup>Guangzhou Ecological and Environmental Monitoring Center of Guangdong  
20 Province, Guangzhou 510060, China

21 <sup>7</sup>State Joint Key Laboratory of Environmental Simulation and Pollution Control,  
22 College of Environmental Sciences and Engineering, Peking University, Beijing  
23 100871, China

24 <sup>8</sup>Institute of Mass Spectrometry and Atmospheric Environment, Guangdong  
25 Provincial Engineering Research Center for on-line Source Apportionment System of  
26 Air Pollution, Jinan University, Guangzhou 510632, China

27 <sup>9</sup>School of Atmospheric Sciences, Sun Yat-Sen University, Guangzhou 510275, China

28 <sup>10</sup>School of Environmental Science and Engineering, Qilu University of Technology,  
29 Jinan 250353, China

30

31 *\*Correspondence to:* Bin Yuan (byuan@jnu.edu.cn) and Min Shao  
32 (mshao@pku.edu.cn)

33

34 **Abstract.** Ambient nitrate has been of increasing concern in PM<sub>2.5</sub>, while there are  
35 still large uncertainties in quantifying the formation of nitrate aerosol. The formation  
36 pathways of nitrate aerosol at an urban site and a suburban site in the Pearl River Delta  
37 (PRD) are investigated using an observation-constrained box model. Throughout the  
38 campaigns, aerosol pollution episodes were constantly accompanied with the increase  
39 of nitrate concentrations and fractions at both urban and suburban sites. The simulations  
40 demonstrate that chemical reactions in the daytime and at night both contributed  
41 significantly to formation of nitrate in the boundary layer at the two sites. However,  
42 nighttime reactions predominately occurred aloft in the residual layer at the urban site  
43 and downward transport from the residual layer in the morning are-is an important  
44 source (53%) for surface nitrate at the urban site, whereas similar amounts of nitrate  
45 were produced in the nocturnal boundary layer and residual layer at the suburban site,  
46 which results in little downward transport of nitrate from the residual layer to the  
47 ground at the suburban site. We show that nitrate formation was in the volatile organic  
48 compounds (VOCs)-limited regime at the urban site, and in the transition regime at the  
49 suburban site, identical to the response of ozone at both sites. The reduction of VOCs  
50 emissions can be an efficient approach to mitigate nitrate in both urban and suburban  
51 areas through influencing hydroxyl radical (OH) and N<sub>2</sub>O<sub>5</sub> production, which will also  
52 be beneficial for the synergistic control of regional ozone pollution. The results  
53 highlight that the relative importance of nitrate formation pathways and ozone can be  
54 site-specific, and the quantitative understanding of various pathways of nitrate  
55 formation will provide insights for developing nitrate and ozone mitigation strategies.

56

57 **Keywords:** nitrate, ozone, volatile organic compounds, N<sub>2</sub>O<sub>5</sub>, formation pathways,  
58 urban and suburban sites

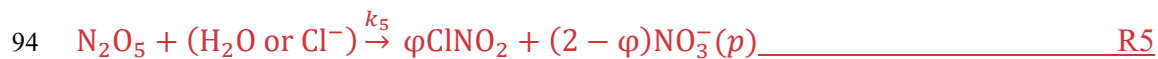
59

## 60 **1 Introduction**

61 Particulate nitrate is a substantial chemical component of fine particles, which  
62 plays a significant role in the acid deposition, visibility reduction, hygroscopic  
63 properties~~property~~, and radiative forcing (Li et al., 1993; Watson, 2002; Pathak et al.,  
64 2009; Xu and Penner, 2012; Zhang et al., 2017; Liu et al., 2020). Due to the larger  
65 emission reduction of SO<sub>2</sub> than NO<sub>x</sub> and little change of NH<sub>3</sub> since the implementation  
66 of the clean air actions in China (Guo et al., 2018; Liu et al., 2019a; Zhai et al., 2021), a  
67 considerable increase in the nitrate fractions in aerosols has been observed in haze  
68 periods in the northern China Plain (Wen et al., 2018; Li et al., 2018; Lu et al., 2013; Fu  
69 et al., 2020), southern China (Pathak et al., 2009; Pathak et al., 2011) and eastern China  
70 (Griffith et al., 2015; Tao et al., 2018; Yun et al., 2018b; Li et al., 2018), which indicates  
71 the growing significance of nitrate in the formation of haze events. In addition, the  
72 photolysis of particulate nitrate can increase the production of sulfate and nitrous acid  
73 (HONO), implying the importance of nitrate in the synergetic enhancement of the  
74 atmospheric oxidizing capability in haze events (Gen et al., 2019; Zhang et al., 2020; Ye  
75 et al., 2016; Ye et al., 2017), although the photolysis of particulate nitrate to produce  
76 HONO still remains highly uncertain (Romer et al., 2018). Hence, identifying and  
77 understanding the driving factors of nitrate formation are essential to establishment of  
78 optimized mitigation policies for fine particles.

79 Particulate inorganic nitrate is primarily produced through two processes: the  
80 photochemical reaction of hydroxyl radical (OH) and NO<sub>2</sub> during daytime (R1) and  
81 the heterogeneous uptake of N<sub>2</sub>O<sub>5</sub> (R2–R5) during nighttime. The gaseous nitric acid  
82 (HNO<sub>3</sub>) is produced by the reaction of OH and NO<sub>2</sub>, and then reacts with ammonia  
83 (NH<sub>3</sub>) to form particulate nitrate (Stelson and Seinfeld, 1982). The partitioning process  
84 of HNO<sub>3</sub> between the gas and particle phase is regulated by ambient temperature (*T*),  
85 relative humidity (RH) (Mozurkewich, 1993), aerosol pH and the abundance of NH<sub>3</sub>  
86 (R7) (Xue et al., 2014a; Yun et al., 2018b; Franchin et al., 2018). The pH value within  
87 a certain range plays an important role in the gas-particle partitioning of nitrate, which  
88 significantly impacts the nitrate formation (Guo et al., 2018; Lawal et al., 2018; Nenes  
89 et al., 2020).





95  $k_5 = \frac{\omega_1 \gamma Sa}{4}$  \_\_\_\_\_ (Eq.1)



97  $k_6 = J_{\text{ClNO}_2}$  \_\_\_\_\_ (Eq.2)



99 The heterogeneous uptake reaction of  $\text{N}_2\text{O}_5$  can occur on the surface of water or  
 100 chlorine-containing particle (R5); and the reaction constant ( $k_5$ ) is described by Eq.1,  
 101 where  $\varphi$  is the production yield of  $\text{ClNO}_2$  in R5,  $\omega_1$  is the average molecular speed of  
 102  $\text{N}_2\text{O}_5$  ( $\text{m s}^{-1}$ ),  $\gamma$  is the uptake coefficient of  $\text{N}_2\text{O}_5$  and  $Sa$  ( $\text{m}^2 \text{m}^{-3}$ ) is the aerosol surface  
 103 area concentration in Eq.1. The nitryl chloride ( $\text{ClNO}_2$ ) produced by the heterogeneous  
 104 uptake reaction of  $\text{N}_2\text{O}_5$  at night would photolysis in the next morning, which would  
 105 produce chlorine atom and  $\text{NO}_2$  (R6). Here the reaction rate  $k_6$  was denoted as the  
 106 photolysis rate of  $\text{ClNO}_2$  ( $J_{\text{ClNO}_2}$ ). The heterogeneous uptake reaction of  $\text{N}_2\text{O}_5$  is  
 107 affected by the uptake coefficient ( $\gamma$ ) and the production yield of  $\text{ClNO}_2$  ( $\varphi$ ) (~~R5~~), which  
 108 cannot be directly measured and are significantly impacted by the aerosol components  
 109 and ambient RH (Bertram and Thornton, 2009; Bian et al., 2017; McDuffie et al.,  
 110 2018a; McDuffie et al., 2018b). Thus, the nocturnal contribution to nitrate formation  
 111 still has great uncertainty.

112 With the radiative cooling in the afternoon, the mixed layer decoupled into a  
 113 steady, near surface nocturnal boundary layer (NBL) and a residual layer (RL), which  
 114 is a neutral layer and formed aloft during the turbulence attenuation process (Prabhakar  
 115 et al., 2017). ~~In addition,~~ Tthe heterogeneous uptake of  $\text{N}_2\text{O}_5$  in the nocturnal boundary  
 116 layer is greatly disturbed in the presence of fresh NO emissions, which titrate the  $\text{NO}_3$   
 117 radical within the stagnant boundary layer (Geyer and Stutz, 2004; Li et al., 2020; Chen  
 118 et al., 2020). However, aircraft observations in California and Utah in the US have  
 119 revealed that active uptake of  $\text{N}_2\text{O}_5$  in the residual layer contributed a major portion of  
 120 the near-surface nitrate accumulation during the morning transport from aloft (Brown  
 121 et al., 2006; Chow et al., 2006; Prabhakar et al., 2017; McDuffie et al., 2019; Womack et

122 al., 2019). Similarly, ground- and tower-based field observations also pointed out the  
123 important contribution of this pathway to the rapid increase of near-surface nitrate  
124 concentrations in Beijing, China (Wang et al., 2018a;Chen et al., 2020). However,  
125 under different atmospheric conditions, the relative importance of nitrate production  
126 varies significantly within the residual layer (McDuffie et al., 2019;Tang et al., 2021),  
127 giving widely varying relative contributions of the major chemical pathways to nitrate  
128 pollution among different sites (Wang et al., 2018a;Womack et al., 2019;Chen et al.,  
129 2020;Lin et al., 2020). A comprehensive understanding of the nitrate production in the  
130 residual layer is required to quantify the contributions of different formation pathways  
131 to nitrate pollution.

132 The nitrate production from the reaction of OH and NO<sub>2</sub> pathway during daytime  
133 is well-understood, and the control of NO<sub>x</sub> emission is commonly considered as an  
134 effective strategy to reduce ambient nitrate. However, several studies reported that the  
135 efficiency of NO<sub>x</sub> reduction in nitrate control is limited, and it may enhance nitrate  
136 production under some conditions (Womack et al., 2019;Dong et al., 2014;Hou et al.,  
137 2019). The study by Womack et al. (2019) showed that both nitrate and ozone were  
138 VOCs-limited in Salt Lake City, suggesting that VOCs control would effectively reduce  
139 nitrate. Similarly, modeling studies also found that the nitrate formation was more  
140 sensitive to the change in VOCs concentrations over the northern and eastern China  
141 (Dong et al., 2014;Lu et al., 2019;Fu et al., 2020). ~~However, T~~the sensitivity of nitrate  
142 production to both NO<sub>x</sub> and VOCs in different regions should be comparatively  
143 evaluated, which could provide helpful implications in formulating effective control  
144 strategies for the mitigation of aerosol pollution.

145 In recent years, the nitrate formation in haze episodes has been studied in northern  
146 China (Liu et al., 2015;Wang et al., 2017a;Wen et al., 2018;Fu et al., 2020;Chen et al.,  
147 2020), eastern China (Tao et al., 2016;Lin et al., 2020) and southern China (Qin et al.,  
148 2017;Tao et al., 2018;Yun et al., 2018b;Su et al., 2020), and the important contribution  
149 of the heterogeneous uptake of N<sub>2</sub>O<sub>5</sub> in the nighttime has been discussed (Wang et al.,  
150 2017b;Yun et al., 2018b;Yun et al., 2018a;Chen et al., 2020). However, these ground-  
151 based observations rarely considered the potential contributions of reactive uptake of  
152 N<sub>2</sub>O<sub>5</sub> aloft in the residual layer, which could be an important source of near-surface  
153 nitrate concentrations. In addition, few studies have comprehensively evaluated the  
154 relative influence of NO<sub>x</sub> and VOCs reductions on nitrate production in the urban and  
155 suburban areas~~different environments~~ (Hou et al., 2019).

156 In this study, we present the results from the ground- and tower-based  
157 measurements in both urban and suburban areas in southern China. An observation-  
158 constrained box model was used to simulate the production rates of nitrate from  
159 different formation pathways, and to compare the effects of reducing NO<sub>x</sub> and VOCs  
160 emissions in both urban and suburban areas. This work provides new insights into the  
161 synergetic mitigation of particle and ozone pollution, which can guide development of  
162 the most effective nitrate control strategies.

## 163 **2 Method and data**

### 164 **2.1 Field observation**

165 The ground-based field measurements were conducted at both an urban site in  
166 Guangzhou and a suburban site in Heshan. The tower-based measurements were  
167 conducted at an urban site in Guangzhou. The ground-based study in Guangzhou was  
168 carried out from late September to mid-November in 2018 at the Institute of  
169 Geochemistry (GIG), Chinese Academy of Sciences (23.1°N, 113.2°E), which is a  
170 typical urban site surrounded by a residential area and traffic avenues (Fig. 1). The  
171 instruments were deployed on the top of the 25-m building at GIG site. The ground-  
172 based measurement at the suburban site was performed from late September to mid-  
173 November in 2019 at the supersite of Heshan county (22.7°N, 112.9°E), which is  
174 approximately 50 km southwest to Foshan and 80 km southwest to Guangzhou, and is  
175 frequently influenced by anthropogenic emissions from upwindward Guangzhou-  
176 Foshan mega-city areas. The tower-based measurements ~~in Guangzhou~~ were conducted  
177 simultaneously at the ground and 448 m on the Canton Tower from late September to  
178 mid-November in 2018 concurrent with the measurements at the GIG site, in  
179 Guangzhou, which ~~is located~~ approximately 5.7 km ~~away from the GIG site~~ apart  
180 each other (Fig. 1).

181 The chemical components of PM<sub>1</sub>, trace gases, and non-methane hydrocarbons  
182 (NMHC), and particle BC content and particle size distribution were both measured at  
183 the GIG and Heshan sites, whereas only trace gases (NO<sub>x</sub> and O<sub>3</sub>) and meteorological  
184 parameters were measured at the Canton Tower site. The non-refractory chemical  
185 compositions of PM<sub>1</sub> (NR-PM<sub>1</sub>), including organics (Org), sulfate (SO<sub>4</sub><sup>2-</sup>), nitrate  
186 (NO<sub>3</sub><sup>-</sup>), ammonium (NH<sub>4</sub><sup>+</sup>), and chloride (Cl<sup>-</sup>) were measured using a high-resolution  
187 time-of-flight aerosol mass spectrometer (HR-ToF-AMS, Aerodyne Research Inc., US)

188 (Hu et al., 2016;Chen et al., 2021). Black carbon (BC) was measured using an  
189 aethalometer (AE33, Magee Scientific Co., US). Particle number size distribution was  
190 measured using a scanning mobility particle sizer with an aerodynamic diameter  
191 ranging from 10 to 650 nm (SMPS, TSI, US) and aerosol particle sizer ranging from  
192 500 nm to 20  $\mu\text{m}$  (APS, TSI, US). [Details on the limit of detection and accuracy of the](#)  
193 [instruments are presented in Table S1~ Table S3.](#)

194  $\text{HNO}_3$ ,  $\text{N}_2\text{O}_5$ , and  $\text{ClNO}_2$  were measured using iodide-time-of-flight chemical  
195 ionization mass spectrometry (Iodide-TOF-CIMS, Aerodyne Research Inc., US) (Wang  
196 et al., 2020b;Ye et al., 2021). The non-methane hydrocarbons (NMHC) were measured  
197 using online GC-MS-FID (Wuhan Tianhong Co., Ltd, China) (Yuan et al., 2012) (Table  
198 [S2S4](#)). The concentrations of oxygenated VOCs (OVOCs), including formaldehyde  
199 (HCHO) and acetaldehyde ( $\text{CH}_3\text{CHO}$ ), [the sum of methyl vinyl ketone \(MVK\) and](#)  
200 [methacrolein \(MACR\)](#) were measured via a high-resolution proton transfer reaction  
201 time-of-flight mass spectrometry (PTR-ToF-MS, Ionicon Analytik, Austria) (Wang et  
202 al., 2020a;Wu et al., 2020). HONO was detected using a long path absorption  
203 photometer (LOPAP) at the GIG site (Yu et al., 2021), and was measured by the gas  
204 and aerosol collector (GAC) instrument at the Heshan site (Dong et al., 2012;Yang et  
205 al., 2014).  $\text{NH}_3$  was also measured by two sets of instruments: a cavity ring-down  
206 spectroscopy (CRDS, Picarro, US) was used at the GIG site and the GAC instrument  
207 was used at the Heshan site (von Bobruzki et al., 2010). [Details on the limit of detection](#)  
208 [and accuracy of the instruments are presented in Table S1.](#)

209 In addition, trace gases ( $\text{O}_3$  (49i),  $\text{NO}_x$  (42i), CO (48i) and  $\text{SO}_2$  (43i)) (Thermo  
210 Scientific, US) and meteorological parameters (i.e., wind speed (WS), wind direction  
211 (WD), temperature ( $T$ ), relative humidity (RH) and pressure ( $P$ )) (Vantage Pro 2, Davis  
212 Instruments Co. , US) were simultaneously measured during these campaigns. The  
213 photolysis frequencies of  $\text{O}_3$ ,  $\text{NO}_2$ , HCHO, and HONO (PFS-100, Focused Photonics  
214 Inc., China) were also measured during the campaigns.

215 Considering the integrity and temporal coverage of the measurements, we mainly  
216 focus on the investigated periods from October 7 to 29, 2018, at the GIG site and from  
217 October 16 to November 16, 2019, at the Heshan site.

## 218 **2.2 Box Model description**

219 A zero-dimensional observation-based box model (F0AM) (Wolfe et al., 2016)  
220 was used to simulate the production of nitrate in this study. The F0AM box model uses  
221 a subset of the Master Chemical Mechanism (MCM) v3.3.1\_ (Saunders et al.,  
222 2003; Jenkin et al., 2003; Bloss et al., 2005), which explicitly describe chemical  
223 reactions of VOCs, RO<sub>x</sub> radicals (including OH, HO<sub>2</sub> and RO<sub>2</sub>), ozone and nitrate, and  
224 was widely used in laboratory and theoretical researches (Edwards et al.,  
225 2017; Anderson et al., 2017; D'Ambro et al., 2017; Womack et al., 2019).

226 In this study, the box model was constrained by observations of NMHCs, HCHO,  
227 CH<sub>3</sub>CHO, NO, CO, CH<sub>4</sub>, HONO, and meteorological parameters (i.e., photolysis rates,  
228 RH, *T* and *P*) measured at the GIG and Heshan sites. To investigate the convection of  
229 nitrate between the residual layer and the surface, the box model was split into two  
230 boxes at night (from 17:00 to 6:00 of the following morning) to separately represent the  
231 nocturnal boundary layer and the residual layer, respectively (Womack et al. (2019)  
232 (Fig. S1).

233 The simulation of the residual layer at the GIG site was constrained by the  
234 observation data from 488 m at the Canton Tower, while the simulation of the residual  
235 layer at the Heshan site was freely evolved from sunset time using the ground  
236 observation data of Heshan. The detailed model settings are described in Text S1, and  
237 the agreement between the observation data and simulations at the GIG and Canton  
238 Tower sites supports the use of similar simulation of the residual layer at the Heshan  
239 site. The model was operated in a time-dependent mode with a 5-min resolution. It was  
240 run for a 72-hour spin-up time to build steady-state concentrations for secondary  
241 pollutants that were not constrained during simulation. To prevent the build-up of long-  
242 lived secondary species to unreasonable levels, an additional physical dilution process  
243 with a lifetime of 24 h was applied in the model (Lu et al., 2017; Decker et al.,  
244 2019; Novak and Bertram, 2020; Liu et al., 2021; Yun et al., 2018b). To achieve  
245 agreement with the observation, a life time of 24 h and 8 h were used at the GIG and  
246 Heshan site, respectively. The sensitivity tests with different dilution constant at the  
247 GIG and Heshan site were shown in Fig.S2 and Fig.S3, respectively. The background  
248 concentrations for ozone and CH<sub>4</sub> were set as 30 ppb and 1.8 ppm, respectively (Wang  
249 et al., 2011).



250 The nocturnal production of nitrate from  $\text{N}_2\text{O}_5$  hydrolysis and the subsequent  
251 reactions (R5 and R6) are added to the box model. ~~The reaction rates of R5 and R6 are~~  
252 ~~expressed as Eqs. 1 and 2, respectively:~~  
253 ~~where  $\bar{c}_1$  is the average molecular speed of  $\text{N}_2\text{O}_5$ ,  $\gamma$  is the uptake coefficient of  $\text{N}_2\text{O}_5$~~   
254 ~~and  $\phi$  is the production yield of  $\text{ClNO}_2$  in R5.~~  $\gamma$  and  $\phi$  are calculated using the new  
255 observation-based empirical parameterization method from Yu et al. (2020), where the  
256 impacts of nitrate, chloride, and aerosol liquid water content (ALWC) were evaluated  
257 to better represent the observed  $\gamma$ . The average values of  $\gamma$  were  $0.018 \pm 0.01$  and  
258  $0.019 \pm 0.01$  at the GIG and Heshan sites, respectively, which were comparable with  
259 ~~these~~ observed mean data of  $\gamma$  ( $0.020 \pm 0.019$ ) at the Heshan site in 2017. The  $\phi$  used  
260 in this study were  $0.18 \pm 0.15$  and  $0.20 \pm 0.23$  at the GIG and Heshan sites, which were  
261 slightly lower than the observed mean data of  $\phi$  at the Heshan site ( $0.31 \pm 0.27$ ) in 2017  
262 (Yu et al., 2020). The chemical compositions of fine particles were not measured at the  
263 Canton Tower site, thus values of  $\gamma$  and  $\phi$  in the residual layer were assigned equal to  
264 those of the nocturnal boundary layer. ~~This may lead to negative deviations for  $\gamma$  and~~  
265 ~~positive deviations for  $\phi$  in the residual layer, as higher RH and lower  $\text{PM}_{2.5}$~~   
266 ~~concentrations were observed in the residual layer (as shown in Fig.S4). The  $\gamma$  and  $\phi$~~   
267 ~~exhibited complicated nonlinear dependence on aerosol composition, aerosol liquid~~  
268 ~~water and RH (Bertram and Thornton, 2009; McDuffie et al., 2019; Yu et al., 2020),~~  
269 ~~such that  $\gamma$  and  $\phi$  has positive and negative dependence with RH, respectively. There~~  
270 ~~was higher RH, and lower chloride at the 488 m site, compared to the ground site of~~  
271 ~~Canton Tower. The nitrate concentration was comparable at the 488 m site to the ground~~  
272 ~~site in the study of Zhou et al. (2020). Combined with the higher RH and lower  $\text{PM}_{2.5}$~~   
273 ~~concentrations in the residual layer in this study (as shown in Fig.S4), we inferred the~~  
274 ~~negative deviations for  $\gamma$  and positive deviations for  $\phi$  in the residual layer.~~ The dry  
275 aerosol surface area concentration ( $S_a$ ) was calculated from the particle number size  
276 distribution and calibrated to the actual atmospheric  $S_a$  using the RH-dependent  
277 hygroscopic growth factor ( $f(\text{RH})$ ). The  $f(\text{RH})$  was estimated from the aerosol  
278 composition measured by AMS and the aerosol liquid water content, which included  
279 the inorganic-associated and organic-associated water. The sum of inorganic-associated  
280 water estimated from ISORROPIA thermodynamic model and organic-associated  
281 water estimated from the dry organic aerosol mass, was used to calculate the growth of  
282 wet matter contributions, as described in the study of McDuffie et al. (2018a). $f(\text{RH})$

283 ~~was calculated using the aerosol compositions measured by AMS and estimated liquid~~  
 284 ~~water by thermodynamic model of ISORROPIA, according to the study conducted by~~  
 285 ~~McDuffie et al. (2018a)~~.  $J_{ClNO_2}$  was scaled from measured NO<sub>2</sub> photolysis frequencies  
 286 divided by a factor of 30 (Riedel et al., 2014).

287 The equilibrium coefficient between HNO<sub>3</sub> and particulate nitrate is incorporated  
 288 into the box model as a pseudo-first-order reaction (Eq.3 and 4) through the equilibrium  
 289 absorption partitioning theory (Jacob, 2000; Yuan et al., 2016):



$$291 \quad k_{8f} = \left( \frac{R_a}{D_g} + \frac{4}{\omega \alpha} \right)^{-1} * S_a \quad \text{(Eq.3)}$$

$$292 \quad k_{8b} = \left( \frac{R_a}{D_g} + \frac{4}{\omega \alpha} \right)^{-1} \frac{S_a}{K_{eq}} \quad \text{(Eq.4)}$$

293 where  $R_a$  is the radius of nitrate particles (m),  $D_g$  is the gas-phase molecular diffusion  
 294 coefficient ( $\text{m}^2 \text{ s}^{-1}$ ),  $\omega$  is the mean molecular speed of HNO<sub>3</sub> ( $\text{m s}^{-1}$ ),  $\alpha$  is the mass  
 295 accommodation coefficient of HNO<sub>3</sub>, and  $K_{eq}$  represents the equilibrium constant of  
 296 HNO<sub>3</sub> and nitrate. These coefficients are the same as those in the chemical aqueous-  
 297 phase radical mechanism (CAPRAM) (Ervens et al., 2003; Wen et al., 2015).

298 The empirical kinetic modeling approach (EKMA) is used here to identify the  
 299 sensitivity of ozone and nitrate to the variations of NO<sub>x</sub> and VOCs. The observed  
 300 diurnal average conditions are used as the input for the base simulation. Sensitivity tests  
 301 are conducted by increasing and decreasing initial anthropogenic VOCs (AVOCs) and  
 302 NO<sub>x</sub> concentrations by a ratio ranging from 0.1 to 2.0 with 20 equal-distance steps  
 303 without changing other parameters in the model (Tan et al., 2018; Lyu et al.,  
 304 2019; Womack et al., 2019). The maximum concentration of ozone and nitrate in each  
 305 scenario are plotted to generate the contour plots of the respective isopleths. Isoprene  
 306 was included in the simulation as biogenic VOC (BVOC). Reducing ~~biogenic VOCs~~  
 307 ~~(BVOCs)~~ such as isoprene is impractical, so ~~they are it is~~ not scaled with AVOCs  
 308 concentrations in the sensitivity simulations on control of precursors.

309 Since the N<sub>2</sub>O<sub>5</sub> is affected by the chemistry between ozone and VOCs,  
 310 ~~constraining~~ N<sub>2</sub>O<sub>5</sub> concentrations with the change in NO<sub>x</sub> ratio arbitrarily during the  
 311 isopleth simulations is meaninglessimproper. Thus, we set the simulation of base case  
 312 (S0) without N<sub>2</sub>O<sub>5</sub> constrained. To evaluate the results of the base case, we design  
 313 another simulation with N<sub>2</sub>O<sub>5</sub> constrained (S1) and we compare the two simulated

314 nitrate ~~with the observation with and without the N<sub>2</sub>O<sub>5</sub> constrained~~ in Fig. S52. ~~The~~  
315 ~~model scenarios were described in Table S5 in detail.~~ The base case simulation (S0)  
316 was comparable to the ~~observation. results without N<sub>2</sub>O<sub>5</sub> constrained.~~ The simulated  
317 nitrate with N<sub>2</sub>O<sub>5</sub> constrained (S1) during October 9 to 10, 2018 was observed to be  
318 much higher compared to both the observations and base case simulation (S0) at the  
319 GIG site, which suggest that high concentrations of ambient N<sub>2</sub>O<sub>5</sub> measured during this  
320 short period may not contribute significantly to nitrate formation (Fig. S63). Overall,  
321 the simulated nitrate of base case without N<sub>2</sub>O<sub>5</sub> constrained agreed well with the  
322 observation suggesting the robustness of the model simulations.

323 Gaussian error propagation was used to evaluate the uncertainties about  
324 measurement parameters and reaction rates in the model performance, as described in  
325 Lu et al. (2012). The uncertainties of various measurement parameters (VOCS, trace  
326 gases, meteorological parameters, etc.) ranged from 0 to 20%, and uncertainties of  
327 reaction rates are in the order of ~20% (Lu et al., 2012), ~~while less than 10% uncertainty~~  
328 ~~is derived from deposition velocity (Lou et al., 2010). Therefore, the uncertainty of~~  
329 ~~simulated results in the base model is estimated to be around 50%.~~  
330 (Guo et al., 2018; Nenes et al., 2020; Fountoukis and Nenes, 2007; Franchin et al., 2018)

## 331 **3 Results and discussion**

### 332 **3.1 Overview of nitrate concentrations during the campaign**

333 The temporal variations of mass concentrations of the major chemical components  
334 in PM<sub>1</sub> are shown in Fig. 2. The mean concentration of PM<sub>1</sub> was 41.7±23.1 μg m<sup>-3</sup> at  
335 the GIG site during the investigated period, which was comparable with that at the  
336 Heshan site (40.6 ±15.5 μg m<sup>-3</sup>). The aerosol composition differed between sites, with  
337 inorganic ions (sulfate, nitrate, and ammonia) higher and organic matter lower at the  
338 GIG site compared to the Heshan site.

339 Although the mass concentrations at the two sites were comparable, the mass  
340 fraction of nitrate in PM<sub>1</sub> at the GIG site increased from 10% to 33% as the mass  
341 concentration of PM<sub>1</sub> increased from 20 to 130 μg m<sup>-3</sup> (Fig. 3), while the fraction of  
342 nitrate increased from 10% to 20% at the Heshan site, suggesting that nitrate plays a  
343 more important role in the increase in PM<sub>1</sub> at the urban site than that at the suburban  
344 site. The significant increasing ratio of nitrate fraction from clean condition to polluted  
345 condition (~ 43%) was also revealed in the airborne observation in Utah Valley, US

346 (Franchin et al., 2018). In addition, although the concentration of sulfate was higher  
347 than that of nitrate during most of the sampling periods, as PM<sub>1</sub> increased the mass  
348 concentration ratio of nitrate/sulfate increased from 0.5 to 2.0 at the GIG site and from  
349 0.5 to 1.5 at the Heshan site. The higher ratios of nitrate/sulfate during the polluted  
350 periods implies that reducing nitrate may be essential for reducing the occurrence of  
351 PM pollution in southern China. The increasing contributions of nitrate to PM<sub>1</sub> in this  
352 study were similar with those observed in northern China during haze pollution (Yang  
353 et al., 2017;Fu et al., 2020;Wen et al., 2015;Liu et al., 2015), suggesting the significance  
354 of nitrate mitigation to further reduce mass concentrations of fine particles in China.

355 The diurnal patterns of mean nitrate, NH<sub>3</sub>, NO<sub>2</sub> and HNO<sub>3</sub> concentrations observed  
356 at the GIG and Heshan sites are shown in Fig. 4. The highest nitrate concentration was  
357 observed in the morning at the GIG site and during nighttime at the Heshan site,  
358 suggesting differences in the processes that dominated the formation of nitrate at the  
359 two sites. At the GIG site, nitrate rapidly increased from 4:00 to 9:00, but the  
360 concentrations of NH<sub>3</sub> and HNO<sub>3</sub> increased slowly, which suggests the minor  
361 contribution of direct production of HNO<sub>3</sub> from the reaction of OH and NO<sub>2</sub>. The  
362 increase of nitrate during this period might be associated with the downward transport  
363 from the residual layer to the ground.~~The concentration of NO<sub>2</sub> exhibited a decreasing~~  
364 ~~trend during the nitrate growth period. As gaseous HNO<sub>3</sub> is mainly produced by the~~  
365 ~~reaction of OH and NO<sub>2</sub>, the accumulation of nitrate after sunrise might largely be~~  
366 ~~attributable to the downward transport from the residual layer to the ground.~~ The diurnal  
367 variations in O<sub>3</sub> and NO<sub>x</sub> measured at the GIG and Canton Tower sites are shown in  
368 Fig. 5. The ground-based observations at the Canton Tower showed similar variation  
369 patterns of O<sub>3</sub> and NO<sub>x</sub> to the GIG site. However, the average concentration of O<sub>3</sub> at  
370 488 m of Canton Tower site was 2.4 times higher than that at the ground-GIG site during  
371 nighttime, and the lower nocturnal concentrations of NO (1.8 ± 0.2 ppb) at the 488 m  
372 site would enhance the production of NO<sub>3</sub> and N<sub>2</sub>O<sub>5</sub> (Wang et al., 2018b;McDuffie et  
373 al., 2019). Therefore, heterogeneous uptake of N<sub>2</sub>O<sub>5</sub> during nighttime may be active at  
374 488 m at urban site, which will be further investigated in Section 3.2. At the Heshan  
375 site, nitrate increased sharply in the early nighttime (before midnight), which may be  
376 attributable to the shallow nocturnal boundary layer or the enhanced nocturnal N<sub>2</sub>O<sub>5</sub>  
377 heterogeneous uptake reactions. Subsequently, there was a significant increase in  
378 nitrate from 7:00 to 9:00. The concentration of NH<sub>3</sub> showed variation pattern that was

379 similar with that of nitrate and increased after 7:00, while the concentrations of HNO<sub>3</sub>  
380 and NO<sub>2</sub> showed a decreasing trend from 7:00 to 9:00 at the Heshan site. The different  
381 growth characteristics of nitrate and the variation patterns of precursors at the two sites  
382 may be related to different formation processes, which will be discussed in detail later.

383 In this study, the wind speeds in the investigated periods at the GIG and Heshan  
384 sites were generally below 2 m s<sup>-1</sup> (Table S3S6), which suggests that regional transport  
385 may have limited contributions to the abundance of nitrate at the observation sites.  
386 Therefore, the discussion of the chemical formation process of nitrate in this study  
387 focuses on local production.

388 The molar ratios of [NH<sub>4</sub><sup>+</sup>] to the sum of 2×[SO<sub>4</sub><sup>2-</sup>]+[NO<sub>3</sub><sup>-</sup>] are calculated (Fig.  
389 S7S) to determine whether there was enough NH<sub>4</sub><sup>+</sup> to neutralize nitrate. The molar ratios  
390 were approximately 1.0 at both GIG and Heshan sites, suggesting both NH<sub>3</sub> and HNO<sub>3</sub>  
391 were crucial precursors for nitrate formation. the presence of sufficient ammonia to  
392 neutralize both nitrate and sulfate. Based on these discussions, we will discuss the NH<sub>3</sub>  
393 effect on the nitrate partitioning firstly by thermodynamic ISORROPIA II model. The  
394 nitrate chemical formation pathways, which is mainly attributable to the production of  
395 HNO<sub>3</sub> and/or heterogeneous uptake of N<sub>2</sub>O<sub>5</sub> combining the box model, will be  
396 discussed in Sec. 3.2. conclude that the nitrate production was mainly attributable to the  
397 production of HNO<sub>3</sub> and/or reactive heterogeneous uptake of N<sub>2</sub>O<sub>5</sub>, which will be  
398 discussed in the subsequent section.

399 The ISORROPIA II model setting is described in Test S2 in detail. The  
400 ISORROPIA II modeled results of nitrate, ammonium, HNO<sub>3</sub>, and NH<sub>3</sub> at the GIG and  
401 Heshan site were displayed in Fig.S8 ~ Fig.S9. The particle-phase nitrate and  
402 ammonium at the GIG site showed a bit overestimation, while the gas-phase HNO<sub>3</sub>,  
403 and NH<sub>3</sub> showed overestimation at the Heshan site. Overall, the simulated components  
404 showed good correlations with the observed concentrations at both sites. We use the  
405 ISORROPIA II model results to evaluate the particle fraction of nitrate in the sum of  
406 HNO<sub>3</sub>+nitrate ( $\epsilon(\text{NO}_3^-)$ ) against aerosol pH. Aerosol pH, which depends on the aerosol  
407 acidity and water content, is calculated by the following equation:

$$408 \text{ pH} = -\log_{10} \frac{1000 H_{air}^+}{ALWC} \quad \text{(Eq.5)}$$

409 where  $H_{air}^+$  ( $\mu\text{g m}^{-3}$ ) is the hydronium concentration of the equilibrium particle and  
410 ALWC ( $\mu\text{g m}^{-3}$ ) is the aerosol water content from ISORROPIA II simulation.

411 The  $\epsilon(\text{NO}_3^-)$  against pH at the GIG and Heshan site are shown in Fig.6. The pH  
412 data are colored by relative humidity and fit to an “s-curve” as in Guo et al. (2018). The  
413 clustering of pH data mainly located between 1~3, and the  $\epsilon(\text{NO}_3^-)$  are sensitive to the  
414 change of pH. To further evaluate the sensitivity of  $\text{NH}_3$  and sulfate on this effect, the  
415 input of total ammonium ( $\text{NH}_x$ , ammonium +  $\text{NH}_3$ ) and sulfate were reduced from 10%  
416 to 90% relative to the ISORROPIA II base model, respectively, while keeping other  
417 parameters constant. The response of simulated nitrate concentration and aerosol pH to  
418 changes in  $\text{NH}_x$  and  $\text{SO}_4^{2-}$  are shown in Fig.7. The nitrate concentration decreased with  
419 the reduction of  $\text{NH}_x$ , and had little variation with the reduction of  $\text{SO}_4^{2-}$  (Fig.7 (a ~ b))  
420 at both sites. Along with the reduction of  $\text{NH}_x$ , the pH values decreased significantly  
421 (Fig.7 (c ~ d)), which caused the further decrease of  $\epsilon(\text{NO}_3^-)$ . The pH values showed a  
422 bit increase with the reduction of  $\text{SO}_4^{2-}$ , which may be caused by that there would be  
423 more available ammonium neutralized the hydronium. It is consistent with the study of  
424 Guo et al. (2018) and Nenes et al. (2020), suggesting the partitioning of nitrate was also  
425 affected by the  $\text{NH}_3$  in the pH values between 1~3. Thus, the control of  $\text{NH}_3$  is effective  
426 for the reduction of nitrate by affecting the partitioning process of nitrate at both GIG  
427 and Heshan site in this study. The partitioning of nitrate increased with the reduction of  
428 sulfate suggests the limited role of sulfate reduction on the mitigation of nitrate.

### 429 **3.2 Contributions of different pathways to nitrate formation**

430 To further investigate the chemical formation pathways of nitrate, which related  
431 to the photochemical and heterogeneous reactions, we adopt the box model results to  
432 simulate the contribution of different pathways to nitrate formation. The temporal  
433 variations in simulated and observed nitrate concentrations at the GIG and Heshan sites  
434 are presented in Fig. 86; simulated and observed nitrate showed similar concentrations  
435 and variation patterns. The diurnal variation of simulated nitrate is compared with the  
436 observation in Fig.S10. The diurnal simulated nitrate was comparable with the  
437 observation at the GIG site, especially when considering the vertical transport from the  
438 residual layer in the morning. Unlike the GIG site, the diurnal simulated nitrate  
439 performed higher in the daytime, and little bit lower in the late nighttime, compared  
440 with the observation. It may be related to the lack of quantitative transport in the box  
441 model. The box model performance was evaluated using the mean bias (MB), index of  
442 agreement (IOA), and correlation coefficient ( $r$ ) (Table S4S7) (Liu et al., 2019b;Lyu et  
443 al., 2017;Wang et al., 2019;Curci et al., 2015). The IOA was larger than 0.7 and  $r$  was

444 larger than 0.5 at both sites, indicating good agreements between simulated and  
445 observed nitrate concentrations. The temporal variations in simulated  $\text{N}_2\text{O}_5$  and  $\text{ClNO}_2$   
446 concentrations were higher than comparable with the observations at the Heshan site as  
447 shown in Fig. S63 (c, d), ~~but~~ the simulated results at the GIG site from October 9 to 10  
448 were significantly lower than the observations (Fig. S63 (a, b)). The abnormally high  
449 observed concentrations of  $\text{N}_2\text{O}_5$  and  $\text{ClNO}_2$  that lasted for short periods (10-30 minutes)  
450 at the GIG site may be caused by transported air masses from upwind regions or vertical  
451 transport without well-mixed with fresh urban NO emissions. Simulation of these near-  
452 instantaneous processes transported to the site using a box model is difficult, as box  
453 model is more suitable to simulate the well-mixed air mass with little transport effects.  
454 However, the simulated nitrate concentrations without observed  $\text{N}_2\text{O}_5$  constrained was  
455 adequately comparable with the observations as shown in Fig. S52, implying the  
456 influence of the instantaneously high concentrations of  $\text{N}_2\text{O}_5$  on nitrate formation was  
457 negligible at the GIG site.

458 Based on these simulation results, we calculated the daily-averaged contributions  
459 of the two different reaction pathways to the nitrate concentration - the daytime  
460 production from  $\text{OH} + \text{NO}_2$  reaction and the nighttime ~~uptake-production of from~~  $\text{N}_2\text{O}_5$   
461 uptake reaction in the nocturnal boundary layer and in the residual layer. ~~Since t~~ The  
462 nitrate produced in the residual layer is only gradually mixed to the surface as the  
463 boundary layer develops during the following morning, while the nitrate contributed to  
464 the boundary layer column concentration always included the ~~uptake of~~  $\text{N}_2\text{O}_5$  uptake in  
465 the residual layer during the whole nighttime (Wang et al., 2018a; Womack et al., 2019).  
466 The calculation methods to determine contribution to the boundary layer column  
467 concentrations and to ground-level nitrate concentrations should be distinguished.

468 To calculate the contribution to the boundary layer column concentration, the  
469 integral of the nitrate production rate from  $\text{N}_2\text{O}_5$  uptake ~~reaction~~ from both the nocturnal  
470 surface layer and the residual layer directly contribute to nitrate column concentrations  
471 layer during the whole nighttime, weighted as 0.4 and 0.6 based on their altitude  
472 fractions of the two layers, respectively. This calculation for the contributions to  
473 column concentration is the same as the methods presented by Wang et al. (2018a) and  
474 Womack et al. (2019). However, to quantify the contribution of nitrate produced from  
475 the residual layer to the ground nitrate concentration, one must account for the dynamic  
476 exchange between the residual layer and the surface-based boundary layer that develops

477 during daytime. The integral time for this dynamic exchange was assumed from 6:00  
478 to 10:00 in the morning. Detailed descriptions of the calculations are provided in Text  
479 [S2-S3](#) in Supplementary Materials. The calculation about partitioning process from OH  
480 and NO<sub>2</sub> reaction in the daytime was the same in the two methods mentioned above,  
481 which was the partition part of the integral of the OH and NO<sub>2</sub> reaction during the  
482 daytime.

483 The contributions of nitrate to the boundary layer column concentration (i.e.  
484 average from ground to 1000 m) are shown in Fig. [97a](#). The contribution [of nitrate](#)  
485 [production rate](#) from N<sub>2</sub>O<sub>5</sub> uptake ~~reaction~~ in the residual layer was 17.9 μg m<sup>-3</sup> day<sup>-1</sup>  
486 at the GIG site, which was much greater than the N<sub>2</sub>O<sub>5</sub> uptake in the nocturnal  
487 boundary layer (0.4 μg m<sup>-3</sup> day<sup>-1</sup>). This [ismay be](#) caused by the fresh NO surface  
488 emissions, which titrate the NO<sub>3</sub> radical and ozone in the nocturnal boundary layer, [as](#)  
489 [the mean NO concentration during the nighttime at the GIG site was 12.1 ppb](#). The  
490 contribution from nocturnal nitrate production in the boundary layer was comparable  
491 with the contribution from OH and NO<sub>2</sub> reaction (13.2 μg m<sup>-3</sup> day<sup>-1</sup>) during the daytime.  
492 In contrast to the GIG site, the contribution of [nitrate production rate from](#) N<sub>2</sub>O<sub>5</sub> uptake  
493 ~~from in~~ the nocturnal boundary layer (6.2 μg m<sup>-3</sup> day<sup>-1</sup>) was comparable with that in the  
494 residual layer (4.4 μg m<sup>-3</sup> day<sup>-1</sup>) at the Heshan site. The similar nitrate concentration  
495 and [production rate from](#) N<sub>2</sub>O<sub>5</sub> ~~uptake production rate~~ between the nocturnal boundary  
496 layer and residual layer in Fig. [S127](#) (c, d) was due to smaller NO emissions at the  
497 Heshan site. The results demonstrate that nocturnal nitrate production plays an  
498 important role in nitrate production in the boundary layer, with nighttime contributions  
499 of 58% at the urban site and 35% at the suburban site.

500 The relative magnitudes of the contributions to the daily-averaged surface nitrate  
501 ~~of nitrate~~ differ somewhat from the contributions to the entire boundary layer. The  
502 contributions from the three major pathways to surface nitrate concentrations at the two  
503 sites are compared in Fig. [97b](#). At the GIG site the [nitrate](#) production ~~of nitrate from rate~~  
504 [from](#) the OH and NO<sub>2</sub> reaction and downward transport from the residual layer were  
505 13.2 μg m<sup>-3</sup> day<sup>-1</sup> and 16.6 μg m<sup>-3</sup> day<sup>-1</sup>, contributing 43% and 53% of ground-level  
506 nitrate concentrations, with a minor contribution (1.1 μg m<sup>-3</sup> day<sup>-1</sup>) from [the production](#)  
507 [of](#) N<sub>2</sub>O<sub>5</sub> uptake in the nocturnal boundary layer. This is similar with the results in  
508 Fig. [97a](#), implying a large nitrate contribution from N<sub>2</sub>O<sub>5</sub> uptake in the residual layer,  
509 but not in the nocturnal boundary layer at the urban site.



510 However, at the suburban Heshan site (Fig. 97b), downward transport from the  
511 residual layer made no contribution to the surface nitrate concentration, which was  
512 smaller than the contribution of nitrate from the residual layer in Fig. 97a. This is due  
513 to the similar nitrate production rate from N<sub>2</sub>O<sub>5</sub> uptake ~~rate~~ between the nocturnal  
514 boundary layer and residual layer (see Fig. S127), inducing ~~gradient~~ negligible  
515 convection between the two layers as the result of small concentration gradient (Brown  
516 et al., 2003; Baasandorj et al., 2017; Prabhakar et al., 2017). The nitrate production rate  
517 from OH and NO<sub>2</sub> reaction (19.9 μg m<sup>-3</sup> day<sup>-1</sup>) and nocturnal N<sub>2</sub>O<sub>5</sub> uptake (15.6 μg m<sup>-3</sup>  
518 day<sup>-1</sup>) were the major nitrate formation pathways, which contributed 56% and 44% to  
519 the surface total nitrate production, respectively. Therefore, the importance of residual  
520 layer contribution to the surface nitrate can vary significantly and should be  
521 comprehensively evaluated in different environments. In addition, the nitrate  
522 contributions to the surface concentrations and boundary layer column concentrations  
523 can also be different in different regions, which should be clarified and distinguished  
524 in future studies.

525 In summary, the N<sub>2</sub>O<sub>5</sub> uptake reaction was active in the residual layer both at urban  
526 and suburban sites, ~~but~~ the downward transport from the residual layer was a significant  
527 contributor to surface nitrate at the urban site, but not at the suburban site. This is  
528 attributable to the titration of the NO<sub>3</sub> radical and ozone by fresh NO emissions during  
529 the stagnant boundary layer at the urban site, resulting in the large difference of nitrate  
530 production between the residual and nocturnal boundary layers. In contrast, at the  
531 suburban site, lower NO emissions favored NO<sub>3</sub> production and heterogeneous uptake  
532 of N<sub>2</sub>O<sub>5</sub> both in the nocturnal boundary layer and the residual layer. The horizontal  
533 transport in the residual layer from nocturnal jets may contribute to the different nitrate  
534 production at urban and suburban sites, which has been discussed in the research of  
535 Chow et al. (2006) and Brown et al. (2006). Due to the limitation of box model, this  
536 issue could be studied by the chemistry transport model in further research.

### 537 **3.3 Control of NO<sub>x</sub> and VOCs as mitigation strategies of nitrate**

538 Overall, the contributions of nitrate from the three major pathways, all involving  
539 NO<sub>x</sub> and ozone, suggest that nitrate formation depends not only on the reactions of NO<sub>x</sub>  
540 but also is closely associated with the VOCs-NO<sub>x</sub>-O<sub>3</sub> chemistry. Therefore, the  
541 influence of both NO<sub>x</sub> and VOCs reduction on nitrate production should be considered  
542 in formulating policies to control aerosol pollution.

543 In this study, we adopted the widely used EKMA approach, generally used for  
544 ozone sensitivity analysis (Edwards et al., 2014;Mazzuca et al., 2016;Xue et al.,  
545 2014b;Wang et al., 2015) to investigate the response of nitrate formation in changing  
546 emissions of VOCs and NO<sub>x</sub>. The dependence of simulated nitrate concentrations with  
547 changing of VOCs and NO<sub>x</sub> concentration allow to construct isopleths of nitrate and  
548 ozone production at the GIG and Heshan sites, as displayed in Fig. 108. The production  
549 of nitrate and ozone were in the VOCs-limited regime at the GIG site, and in the  
550 transition regime at the Heshan site, where nitrate and ozone are sensitive to both VOCs  
551 and NO<sub>x</sub> reduction. As shown in Fig. 119, ~~an initial~~ the reduction of NO<sub>x</sub> emissions  
552 from 0 ~ 70% would increase nitrate and ozone concentrations at the GIG site, but  
553 decrease those concentrations at the Heshan site. ~~The An initial~~ decrease in VOCs  
554 concentrations would decrease nitrate and ozone concentrations at both sites. These  
555 results suggest that control of VOCs emissions will efficiently reduce nitrate and ozone  
556 production in both urban and suburban areas, but control of NO<sub>x</sub> emissions will give  
557 different responses between urban and suburban area for both ozone and nitrate. Fig.  
558 119 show that the nitrate sensitivity to the reduction of VOCs and NO<sub>x</sub> emissions was  
559 identical to the response of ozone at both sites. These results demonstrate the possibility  
560 of synergetic control for nitrate and ozone at both urban and suburban sites through  
561 VOCs control.

562 The accuracy of the isopleth plots in Fig. 108 depends on several variables and  
563 parameters included in the box model. Figs S138–149 show the results of simulation  
564 experiments on the dependence of the isopleths upon changing various  
565 parameterization for estimating HONO concentrations, N<sub>2</sub>O<sub>5</sub> uptake coefficient, and  
566 ClNO<sub>2</sub> yields as described in Text S3S4. The sensitivity regime of nitrate and ozone did  
567 not change, although the peak concentrations of ozone and nitrate did change, which  
568 supports the reliability of the results discussed above.

569 As nitrate and ozone exhibit similar sensitivity to the reduction of NO<sub>x</sub> and VOCs,  
570 different VOCs/NO<sub>x</sub> ratios may point to different control strategies. In the cases of the  
571 Heshan and GIG sites, the reduction of NO<sub>x</sub> can adequately control nitrate production  
572 with a VOCs/NO<sub>x</sub> ratio of 1.8 at the Heshan site, while a contrary result can be found  
573 at the GIG site (with a VOCs/NO<sub>x</sub> ratio of 0.8) with a less than 70% reduction of NO<sub>x</sub>  
574 emission in the initial stage. The simulated results at the GIG site agree well with those  
575 reported in the urban areas of Shanghai in China (Dong et al., 2014) and the Salt Lake  
576 City and San Joaquin Valley in the US (Betty and Christian, 2001;Womack et al., 2019),

577 which all emphasized the decrease of nitrate production with the reduction of VOCs  
578 emissions, and the enhanced nitrate production with NO<sub>x</sub> reduction. The results at the  
579 Heshan site were consistent with the simulations at the suburban site of northern China,  
580 where a higher VOCs/NO<sub>x</sub> ratio was found (Wen et al., 2018; Lu et al., 2019). The  
581 synergetic reduction of NO<sub>x</sub> and VOCs is necessary to effectively mitigate the nitrate  
582 production in consideration of the different VOCs/NO<sub>x</sub> ratios in the urban and suburban  
583 areas.

584 The above discussions revealed that direct reduction of NO<sub>x</sub> may not lead to a  
585 decrease in nitrate production. Meanwhile, the reduction of VOCs is effective to  
586 mitigate nitrate production, though they were not the direct precursors of nitrate. To  
587 illustrate these findings, the impacts of changing VOCs and NO<sub>x</sub> on the production rate  
588 of the OH radical, and the rate of OH plus NO<sub>2</sub>, and the N<sub>2</sub>O<sub>5</sub> uptake reaction were  
589 evaluated. During daytime nitrate production involves OH production and its  
590 subsequent reaction with NO<sub>2</sub>. As shown in Fig. 129, the NO<sub>x</sub>-saturated condition at  
591 the GIG site provided sufficient NO<sub>2</sub> to quench the OH radical during daytime. A less  
592 than 70%Initial reduction of NO<sub>x</sub> will increase ozone production and thereby drive  
593 more production of OH, leading to increase in the OH and NO<sub>2</sub> reaction rates. When  
594 NO<sub>x</sub> is lower than 30% of the base case emissions, ozone production would decrease  
595 and lead to the decrease of OH production and its reaction with NO<sub>2</sub>, which in turn  
596 bring about a decrease in nitrate production. In contrast, at the Heshan site, the base  
597 case NO<sub>x</sub> concentrations are lower, giving a production rate of OH that is already  
598 sensitive to both NO<sub>x</sub> and VOCs reductions. The model results indicates that further  
599 emission reductions in both NO<sub>x</sub> and VOCs will simultaneously mitigate the production  
600 of nitrate and ozone.

601 During nighttime, the initial ozone concentration participated the nocturnal  
602 chemistry increased/decreased with the reduction of NO<sub>x</sub> at the GIG/Heshan site. In  
603 addition, the decrease in NO<sub>x</sub> will reduce the titration effect of NO on NO<sub>3</sub> radical and  
604 ozone at the GIG site, which enhances production of N<sub>2</sub>O<sub>5</sub> and promotes nitrate  
605 production in both the nocturnal boundary layer and the residual layer (Fig. 134).  
606 However, at the Heshan site, the reduction of NO<sub>x</sub> cuts down the sources of NO<sub>2</sub> and  
607 NO<sub>3</sub>, decreasing the formation of N<sub>2</sub>O<sub>5</sub> and thus its heterogeneous uptake to produce  
608 nitrate. The reduction of VOCs decreases ozone formation during daytime, thus  
609 attenuating the nocturnal formation of NO<sub>3</sub>, N<sub>2</sub>O<sub>5</sub> and nitrate at both the GIG and  
610 Heshan sites.

611 In summary, nitrate and ozone show similar responses to the reduction of NO<sub>x</sub> and  
612 VOCs for both daytime and nighttime chemical processes, as the result of the coupling  
613 between the formation reactions of ozone and nitrate. The results of this study  
614 emphasize the complex effects of reductions of NO<sub>x</sub> emissions on nitrate concentrations  
615 in the urban and suburban areas. In addition, the ~~initial~~ reduction of VOCs emissions  
616 would be effective in the concurrent mitigation of ozone and nitrate, suggesting that the  
617 reduction of VOCs at present is an effective method for the synergistic control of ozone  
618 and PM<sub>2.5</sub> at present. As there are limitations of box modeling, a comprehensive three-  
619 dimensional model assessment is needed on a regional scale.

## 620 **4 Conclusions**

621 In this study, we use an observation-constrained box model to explore the nitrate  
622 formation pathways and implications for nitrate mitigation strategies at urban and  
623 suburban sites. At both sites, the mass fraction of nitrate in PM<sub>1</sub> increased as the  
624 absolute PM<sub>1</sub> levels increased (from 10% to 33% at the urban site and from 10% to 20%  
625 at the suburban site), suggesting the important role played by nitrate in increasing  
626 particle concentrations in the PRD.

627 Both HNO<sub>3</sub> and NH<sub>3</sub> are important precursors for nitrate formation. Combined  
628 with the ISORROPIA II thermodynamic model, the reduction of NH<sub>3</sub> is effective for  
629 the nitrate reduction by affecting the partitioning process of nitrate at both GIG and  
630 Heshan site. The box model simulations demonstrate that chemical reactions in the  
631 daytime and at night both contributed significantly to formation of nitrate in the  
632 boundary layer at the two sites, with nighttime contributions of 58% at the urban site  
633 and 35% at the suburban site. However, nighttime reactions predominately occurred  
634 aloft in the residual layer at the urban site and downward transport from the residual  
635 layer in the morning are important source (53%) for surface nitrate at the urban site,  
636 whereas similar amounts of nitrate were produced in the nocturnal boundary layer and  
637 residual layer at the suburban site, which results in little downward transport of nitrate  
638 from the residual layer to the ground at this region. The spatial differences of nocturnal  
639 reactions and the ~~opposite-different~~ contributions from downward transport of the  
640 residual layer to surface nitrate at urban and suburban sites were attributed to different  
641 fresh emissions and concentration levels of NO<sub>x</sub> at the two sites during the night time,  
642 suggesting that nitrate production under different NO<sub>x</sub> conditions should be explored to  
643 better understand the its formation pathways.

644 The non-linear relationships between nitrate and  $\text{NO}_x$ , VOCs was developed to  
645 investigate the nitrate mitigation strategies. The simulations demonstrated that the  
646 formation processes of both nitrate and ozone were in the VOCs-limited region at the  
647 urban site and in the transition region at the suburban site. The same sensitivity regimes  
648 of nitrate and ozone at two sites was caused by the similar chemical processes that  
649 account to produce nitrate and ozone. These results suggest that control of VOCs  
650 emissions would effectively mitigate nitrate in both urban and suburban areas.

651 Overall, the formation processes of nitrate are systematically investigated in both  
652 urban and suburban areas in this study, which provides the opportunity to identify  
653 different influencing factors of nitrate production in different environments and offers  
654 insights into the comprehensive mitigation of nitrate pollution in regional scale.  $\text{NO}_x$   
655 emission controls alone might not be an effective strategy for reducing the nitrate  
656 production, while the reduction of VOCs emissions would take effect in the concurrent  
657 mitigation of ozone and nitrate. Thus, an emission control policy focusing on VOCs  
658 will be an effective means for the synergistic control of ozone and  $\text{PM}_{2.5}$  at present. In  
659 the long-term, multi-pollutant control should be implemented to achieve better control  
660 strategies for ozone and  $\text{PM}_{2.5}$ . As the result of limitation for the 0-D box model, vertical  
661 transport and horizontal transport cannot be considered explicitly in this study. Given  
662 the limitations of the box model, three-dimensional models should be used to further  
663 investigate the synergistic control of ozone and particles on the regional scale.

## 664 **Data availability**

665 The observational data used in this study are available from corresponding authors  
666 upon request (byuan@jnu.edu.cn)

## 667 **Author contributions**

668 BY and MS designed the research. SXY, YWP, SH, WC, WWH, CLP, CMW,  
669 ZLW, TGL, EZ, MFC, XBL, SHW, CHW, WWJ, CSY, WS and PC contributed to data  
670 collection. SXY performed the data analysis, with contributions from JZ, DD. Parrish,  
671 XJH, CCL, XYY, YS, HCW, DHC, XMW, ZYZ, JYZ and XMW. SXY and BY  
672 prepared the manuscript with contributions from the other authors. All the authors  
673 reviewed the manuscript.

674 **Competing interests**

675 The authors declare that they have no known competing financial interests or personal  
676 relationships that could have appeared to influence the work reported in this paper.

677 **Acknowledgments**

678 This work was supported by the National Key R&D Plan of China (grant No.  
679 2019YFE0106300, 2018YFC0213904, 2016YFC0202206), the National Natural  
680 Science Foundation of China (grant No. 41877302), the National Natural Science  
681 Foundation of China (grant No. 41905111), Guangdong Natural Science Funds for  
682 Distinguished Young Scholar (grant No. 2018B030306037), Key-Area Research and  
683 Development Program of Guangdong Province (grant No. 2019B110206001),  
684 Guangdong Soft Science Research Program (2019B101001005), and Guangdong  
685 Innovative and Entrepreneurial Research Team Program (grant No. 2016ZT06N263).  
686 This work was also supported by Special Fund Project for Science and Technology  
687 Innovation Strategy of Guangdong Province (Grant No.2019B121205004).

688 **References**

689 Anderson, D. C., Nicely, J. M., Wolfe, G. M., Hanisco, T. F., Salawitch, R. J., Canty, T. P.,  
690 Dickerson, R. R., Apel, E. C., Baidar, S., Bannan, T. J., Blake, N. J., Chen, D., Dix, B.,  
691 Fernandez, R. P., Hall, S. R., Hornbrook, R. S., Gregory Huey, L., Josse, B., Jöckel, P.,  
692 Kinnison, D. E., Koenig, T. K., Le Breton, M., Marécal, V., Morgenstern, O., Oman, L. D.,  
693 Pan, L. L., Percival, C., Plummer, D., Revell, L. E., Rozanov, E., Saiz-Lopez, A., Stenke, A.,  
694 Sudo, K., Tilmes, S., Ullmann, K., Volkamer, R., Weinheimer, A. J., and Zeng, G.:  
695 Formaldehyde in the Tropical Western Pacific: Chemical Sources and Sinks, Convective  
696 Transport, and Representation in CAM-Chem and the CCM1 Models, *Journal of Geophysical*  
697 *Research: Atmospheres*, 122, 11,201-211,226, <https://doi.org/10.1002/2016JD026121>, 2017.  
698 Baasandorj, M., Hoch, S. W., Bares, R., Lin, J. C., Brown, S. S., Millet, D. B., Martin, R.,  
699 Kelly, K., Zarzana, K. J., Whiteman, C. D., Dube, W. P., Tonnesen, G., Jaramillo, I. C., and  
700 Sohl, J.: Coupling between Chemical and Meteorological Processes under Persistent Cold-Air  
701 Pool Conditions: Evolution of Wintertime PM<sub>2.5</sub> Pollution Events and N<sub>2</sub>O<sub>5</sub> Observations in  
702 Utah's Salt Lake Valley, *Environmental Science & Technology*, 51, 5941-5950,  
703 [10.1021/acs.est.6b06603](https://doi.org/10.1021/acs.est.6b06603), 2017.  
704 Bertram, T., and Thornton, J.: Toward a general parameterization of N<sub>2</sub>O<sub>5</sub> reactivity on  
705 aqueous particles: The competing effects of particle liquid water, nitrate and chloride,  
706 *Atmospheric Chemistry and Physics Discussions*, 9, 15181-15214, 2009.

707 Betty, P., and Christian: Sensitivity of particulate matter nitrate formation to precursor  
708 emissions in the California San Joaquin Valley, *Environmental Science & Technology*, 35,  
709 2979-2987, 2001.

710 Bian, H., Chin, M., Hauglustaine, D. A., Schulz, M., Myhre, G., Bauer, S. E., Lund, M. T.,  
711 Karydis, V. A., Kucsera, T. L., Pan, X., Pozzer, A., Skeie, R. B., Steenrod, S. D., Sudo, K.,  
712 Tsigaridis, K., Tsimpidi, A. P., and Tsyro, S. G.: Investigation of global particulate nitrate  
713 from the AeroCom phase III experiment, *Atmos. Chem. Phys.*, 17, 12911-12940,  
714 10.5194/acp-17-12911-2017, 2017.

715 Bloss, C., Wagner, V., Jenkin, M. E., Volkamer, R., Bloss, W. J., Lee, J. D., Heard, D. E.,  
716 Wirtz, K., Martin-Reviejo, M., Rea, G., Wenger, J. C., and Pilling, M. J.: Development of a  
717 detailed chemical mechanism (MCMv3.1) for the atmospheric oxidation of aromatic  
718 hydrocarbons, *Atmos. Chem. Phys.*, 5, 641-664, 10.5194/acp-5-641-2005, 2005.

719 Brown, S. G., Hyslop, N. P., Roberts, P. T., McCarthy, M. C., and Lurmann, F. W.: Wintertime  
720 Vertical Variations in Particulate Matter (PM) and Precursor Concentrations in the San  
721 Joaquin Valley during the California Regional Coarse PM/Fine PM Air Quality Study, *Journal*  
722 *of the Air & Waste Management Association*, 56, 1267-1277,  
723 10.1080/10473289.2006.10464583, 2006.

724 Brown, S. S., Stark, H., Ryerson, T. B., Williams, E. J., Nicks Jr., D. K., Trainer, M.,  
725 Fehsenfeld, F. C., and Ravishankara, A. R.: Nitrogen oxides in the nocturnal boundary layer:  
726 Simultaneous in situ measurements of NO<sub>3</sub>, N<sub>2</sub>O<sub>5</sub>, NO<sub>2</sub>, NO, and O<sub>3</sub>, *Journal of*  
727 *Geophysical Research: Atmospheres*, 108, 10.1029/2002jd002917, 2003.

728 Chen, W., Ye, Y., Hu, W., Zhou, H., Pan, T., Wang, Y., Song, W., Song, Q., Ye, C., Wang, C.,  
729 Wang, B., Huang, S., Yuan, B., Zhu, M., Lian, X., Zhang, G., Bi, X., Jiang, F., Liu, J.,  
730 Canonaco, F., Prevot, A. S. H., Shao, M., and Wang, X.: Real-time characterization of aerosol  
731 compositions, sources and aging processes in Guangzhou during PRIDE-GBA 2018  
732 campaign, *Journal of Geophysical Research: Atmospheres*, n/a, e2021JD035114,  
733 <https://doi.org/10.1029/2021JD035114>, 2021.

734 Chen, X., Wang, H., Lu, K., Li, C., Zhai, T., Tan, Z., Ma, X., Yang, X., Liu, Y., Chen, S.,  
735 Dong, H., Li, X., Wu, Z., Hu, M., Zeng, L., and Zhang, Y.: Field Determination of Nitrate  
736 Formation Pathway in Winter Beijing, *Environmental Science & Technology*,  
737 10.1021/acs.est.0c00972, 2020.

738 Chow, J. C., Chen, L. W. A., Watson, J. G., Lowenthal, D. H., Magliano, K. A., Turkiewicz,  
739 K., and Lehrman, D. E.: PM<sub>2.5</sub> chemical composition and spatiotemporal variability during  
740 the California Regional PM<sub>10</sub>/PM<sub>2.5</sub> Air Quality Study (CRPAQS), *Journal of Geophysical*  
741 *Research: Atmospheres*, 111, 2006.

742 Curci, G., Ferrero, L., Tuccella, P., Barnaba, F., Angelini, F., Bolzacchini, E., Carbone, C., Der  
743 Gon, H. A. C. D. V., Facchini, M. C., and Gobbi, G. P.: How much is particulate matter near

744 the ground influenced by upper-level processes within and above the PBL? A summertime  
745 case study in Milan (Italy) evidences the distinctive role of nitrate, *Atmospheric Chemistry  
746 and Physics*, 15, 2629-2649, 2015.

747 D'Ambro, E. L., Møller, K. H., Lopez-Hilfiker, F. D., Schobesberger, S., Liu, J., Shilling, J.  
748 E., Lee, B. H., Kjaergaard, H. G., and Thornton, J. A.: Isomerization of Second-Generation  
749 Isoprene Peroxy Radicals: Epoxide Formation and Implications for Secondary Organic  
750 Aerosol Yields, *Environmental Science & Technology*, 51, 4978-4987,  
751 10.1021/acs.est.7b00460, 2017.

752 Decker, Z. C. J., Zarzana, K. J., Coggon, M., Min, K.-E., Pollack, I., Ryerson, T. B., Peischl,  
753 J., Edwards, P., Dubé, W. P., Markovic, M. Z., Roberts, J. M., Veres, P. R., Graus, M.,  
754 Warneke, C., de Gouw, J., Hatch, L. E., Barsanti, K. C., and Brown, S. S.: Nighttime  
755 Chemical Transformation in Biomass Burning Plumes: A Box Model Analysis Initialized with  
756 Aircraft Observations, *Environmental Science & Technology*, 53, 2529-2538,  
757 10.1021/acs.est.8b05359, 2019.

758 Dong, H. B., Zeng, L. M., Hu, M., Wu, Y. S., Zhang, Y. H., Slanina, J., Zheng, M., Wang, Z.  
759 F., and Jansen, R.: Technical Note: The application of an improved gas and aerosol collector  
760 for ambient air pollutants in China, *Atmos. Chem. Phys.*, 12, 10519-10533, 10.5194/acp-12-  
761 10519-2012, 2012.

762 Dong, X., Li, J., Fu, J. S., Gao, Y., Huang, K., and Zhuang, G.: Inorganic aerosols responses  
763 to emission changes in Yangtze River Delta, China, *Science of The Total Environment*, 481,  
764 522-532, 2014.

765 Edwards, P., Aikin, K. C., Dube, W. P., Fry, J. L., Gilman, J. B., De Gouw, J. A., Graus, M.,  
766 Hanisco, T. F., Holloway, J. S., and Hubler, G.: Transition from high- to low-NO<sub>x</sub> control of  
767 night-time oxidation in the southeastern US, *Nature Geoscience*, 10, 490-495, 2017.

768 Edwards, P. M., Brown, S. S., Roberts, J. M., Ahmadov, R., Banta, R. M., deGouw, J. A.,  
769 Dubé, W. P., Field, R. A., Flynn, J. H., Gilman, J. B., Graus, M., Helmig, D., Koss, A.,  
770 Langford, A. O., Lefer, B. L., Lerner, B. M., Li, R., Li, S.-M., McKeen, S. A., Murphy, S. M.,  
771 Parrish, D. D., Senff, C. J., Soltis, J., Stutz, J., Sweeney, C., Thompson, C. R., Trainer, M. K.,  
772 Tsai, C., Veres, P. R., Washenfelder, R. A., Warneke, C., Wild, R. J., Young, C. J., Yuan, B.,  
773 and Zamora, R.: High winter ozone pollution from carbonyl photolysis in an oil and gas  
774 basin, *Nature*, 514, 351, 10.1038/nature13767, 2014.

775 Ervens, B., George, C., Williams, J. E., Buxton, G. V., Salmon, G. A., Bydder, M., Wilkinson,  
776 F., Dentener, F., Mirabel, P., Wolke, R., and Herrmann, H.: CAPRAM 2.4 (MODAC  
777 mechanism): An extended and condensed tropospheric aqueous phase mechanism and its  
778 application, *Journal of Geophysical Research: Atmospheres*, 108, 10.1029/2002JD002202,  
779 2003.

780 Fountoukis, C., and Nenes, A.: ISORROPIA II: a computationally efficient thermodynamic



781 equilibrium model for  $K^+$ - $Ca^{2+}$ - $Mg^{2+}$ - $NH_4^+$ - $Na^+$ - $SO_4^{2-}$ - $NO_3^-$ - $Cl^-$ - $H_2O$  aerosols  
782 aerosols, *Atmos. Chem. Phys.*, 7, 4639-4659, 10.5194/acp-7-4639-2007, 2007.

783 Franchin, A., Fibiger, D. L., Goldberger, L., McDuffie, E. E., Moravek, A., Womack, C. C.,  
784 Crosman, E. T., Docherty, K. S., Dube, W. P., Hoch, S. W., Lee, B. H., Long, R., Murphy, J.  
785 G., Thornton, J. A., Brown, S. S., Baasandorj, M., and Middlebrook, A. M.: Airborne and  
786 ground-based observations of ammonium-nitrate-dominated aerosols in a shallow boundary  
787 layer during intense winter pollution episodes in northern Utah, *Atmos. Chem. Phys.*, 18,  
788 17259-17276, 10.5194/acp-18-17259-2018, 2018.

789 Fu, X., Wang, T., Gao, J., Wang, P., Liu, Y., Wang, S., Zhao, B., and Xue, L.: Persistent Heavy  
790 Winter Nitrate Pollution Driven by Increased Photochemical Oxidants in Northern China,  
791 *Environmental Science & Technology*, 54, 3881-3889, 10.1021/acs.est.9b07248, 2020.

792 Gen, M., Zhang, R., Huang, D. D., Li, Y., and Chan, C. K.: Heterogeneous  $SO_2$  Oxidation in  
793 Sulfate Formation by Photolysis of Particulate Nitrate, *Environmental Science & Technology*  
794 *Letters*, 6, 86-91, 10.1021/acs.estlett.8b00681, 2019.

795 Geyer, A., and Stutz, J.: Vertical profiles of  $NO_3$ ,  $N_2O_5$ ,  $O_3$ , and  $NO_x$  in the nocturnal  
796 boundary layer: 2. Model studies on the altitude dependence of composition and chemistry,  
797 *Journal of Geophysical Research*, 109, 2004.

798 Griffith, S. M., Huang, X. H. H., Louie, P. K. K., and Yu, J. Z.: Characterizing the  
799 thermodynamic and chemical composition factors controlling  $PM_{2.5}$  nitrate: Insights gained  
800 from two years of online measurements in Hong Kong, *Atmospheric Environment*, 122, 864-  
801 875, <https://doi.org/10.1016/j.atmosenv.2015.02.009>, 2015.

802 Guo, H., Otjes, R., Schlag, P., Kiendler-Scharr, A., Nenes, A., and Weber, R. J.: Effectiveness  
803 of ammonia reduction on control of fine particle nitrate, *Atmos. Chem. Phys.*, 18, 12241-  
804 12256, 10.5194/acp-18-12241-2018, 2018.

805 Hou, X., Chan, C., Dong, G., and Yim, S.: Impacts of transboundary air pollution and local  
806 emissions on  $PM_{2.5}$  pollution in the Pearl River Delta region of China and the public health,  
807 and the policy implications, *Environmental Research Letters*, 14, 034005, 2019.

808 Hu, W., Hu, M., Hu, W., Jimenez, J. L., Yuan, B., Chen, W., Wang, M., Wu, Y., Chen, C.,  
809 Wang, Z., Peng, J., Zeng, L., and Shao, M.: Chemical composition, sources, and aging  
810 process of submicron aerosols in Beijing: Contrast between summer and winter, *Journal of*  
811 *Geophysical Research: Atmospheres*, 121, 1955-1977, 10.1002/2015JD024020, 2016.

812 Jacob, D. J.: Heterogeneous chemistry and tropospheric ozone, *Atmospheric Environment*,  
813 34, 2131-2159, [http://dx.doi.org/10.1016/S1352-2310\(99\)00462-8](http://dx.doi.org/10.1016/S1352-2310(99)00462-8), 2000.

814 Jenkin, M. E., Saunders, S. M., Wagner, V., and Pilling, M. J.: Protocol for the development  
815 of the Master Chemical Mechanism, MCM v3 (Part B): tropospheric degradation of aromatic  
816 volatile organic compounds, *Atmos. Chem. Phys.*, 3, 181-193, 10.5194/acp-3-181-2003,  
817 2003.

818 Lawal, A. S., Guan, X., Liu, C., Henneman, L. R. F., Vasilakos, P., Bhogineni, V., Weber, R.  
819 J., Nenes, A., and Russell, A. G.: Linked Response of Aerosol Acidity and Ammonia to SO<sub>2</sub>  
820 and NO<sub>x</sub> Emissions Reductions in the United States, *Environmental Science & Technology*,  
821 52, 9861-9873, 10.1021/acs.est.8b00711, 2018.

822 Li, H., Zhang, Q., Zheng, B., Chen, C., Wu, N., Guo, H., Zhang, Y., Zheng, Y., Li, X., and He,  
823 K.: Nitrate-driven urban haze pollution during summertime over the North China Plain,  
824 *Atmos. Chem. Phys.*, 18, 5293-5306, 10.5194/acp-18-5293-2018, 2018.

825 Li, L., Lu, C., Chan, P.-W., Zhang, X., Yang, H.-L., Lan, Z.-J., Zhang, W.-H., Liu, Y.-W., Pan,  
826 L., and Zhang, L.: Tower observed vertical distribution of PM<sub>2.5</sub>, O<sub>3</sub> and NO<sub>x</sub> in the Pearl  
827 River Delta, *Atmospheric Environment*, 220, 117083,  
828 <https://doi.org/10.1016/j.atmosenv.2019.117083>, 2020.

829 Li, S. M., Anlauf, K., and Wiebe, H.: Heterogeneous nighttime production and deposition of  
830 particle nitrate at a rural site in North America during summer 1988, *Journal of Geophysical*  
831 *Research: Atmospheres*, 98, 5139-5157, 1993.

832 Lin, Y. C., Zhang, Y. L., Fan, M. Y., and Bao, M.: Heterogeneous formation of particulate  
833 nitrate under ammonium-rich regimes during the high-PM<sub>2.5</sub> events in Nanjing, China,  
834 *Atmos. Chem. Phys.*, 20, 3999-4011, 10.5194/acp-20-3999-2020, 2020.

835 Liu, J., Ren, C., Huang, X., Nie, W., Wang, J., Sun, P., Chi, X., and Ding, A.: Increased  
836 Aerosol Extinction Efficiency Hinders Visibility Improvement in Eastern China, *Geophysical*  
837 *Research Letters*, 47, e2020GL090167, <https://doi.org/10.1029/2020GL090167>, 2020.

838 Liu, J., Liu, Z., Ma, Z., Yang, S., Yao, D., Zhao, S., Hu, B., Tang, G., Sun, J., Cheng, M., Xu,  
839 Z., and Wang, Y.: Detailed budget analysis of HONO in Beijing, China: Implication on  
840 atmosphere oxidation capacity in polluted megacity, *Atmospheric Environment*, 244, 117957,  
841 <https://doi.org/10.1016/j.atmosenv.2020.117957>, 2021.

842 Liu, M., Huang, X., Song, Y., Tang, J., Cao, J., Zhang, X., Zhang, Q., Wang, S., Xu, T., Kang,  
843 L., Cai, X., Zhang, H., Yang, F., Wang, H., Yu, J. Z., Lau, A. K. H., He, L., Huang, X., Duan,  
844 L., Ding, A., Xue, L., Gao, J., Liu, B., and Zhu, T.: Ammonia emission control in China  
845 would mitigate haze pollution and nitrogen deposition, but worsen acid rain, *Proceedings of*  
846 *the National Academy of Sciences*, 116, 7760, 10.1073/pnas.1814880116, 2019a.

847 Liu, X., Sun, K., Qu, Y., Hu, M., Sun, Y., Zhang, F., and Zhang, Y.: Secondary formation of  
848 sulfate and nitrate during a haze episode in megacity Beijing, China, *Aerosol Air Qual. Res.*,  
849 15, 2246-2257, 2015.

850 Liu, X., Lyu, X., Wang, Y., Jiang, F., and Guo, H.: Intercomparison of O<sub>3</sub> formation and  
851 radical chemistry in the past decade at a suburban site in Hong Kong, *Atmos. Chem. Phys.*,  
852 19, 5127-5145, 10.5194/acp-19-5127-2019, 2019b.

853 Lou, S., Holland, F., Rohrer, F., Lu, K., Bohn, B., Brauers, T., Chang, C., Fuchs, H., Häsel, R.,  
854 and Kita, K.: Atmospheric OH reactivities in the Pearl River Delta-China in summer 2006:

855 measurement and model results, *Atmospheric Chemistry and Physics*, 10, 11243, 2010.

856 Lu, K., Rohrer, F., Holland, F., Fuchs, H., Bohn, B., Brauers, T., Chang, C., Häseler, R., Hu,  
857 M., and Kita, K.: Observation and modelling of OH and HO<sub>2</sub> concentrations in the Pearl  
858 River Delta 2006: a missing OH source in a VOC rich atmosphere, *Atmospheric chemistry  
859 and physics*, 12, 1541, 2012.

860 Lu, K., Fuchs, H., Hofzumahaus, A., Tan, Z., Wang, H., Zhang, L., Schmitt, S. H., Rohrer, F.,  
861 Bohn, B., Broch, S., Dong, H., Gkatzelis, G. I., Hohaus, T., Holland, F., Li, X., Liu, Y., Liu,  
862 Y., Ma, X., Novelli, A., Schlag, P., Shao, M., Wu, Y., Wu, Z., Zeng, L., Hu, M., Kiendler-  
863 Scharr, A., Wahner, A., and Zhang, Y.: Fast Photochemistry in Wintertime Haze:  
864 Consequences for Pollution Mitigation Strategies, *Environmental Science & Technology*,  
865 10.1021/acs.est.9b02422, 2019.

866 Lu, K. D., Hofzumahaus, A., Holland, F., Bohn, B., Brauers, T., Fuchs, H., Hu, M., seler, R.  
867 H., Kita, K., Kondo, Y., Li, X., Lou, S. R., Oebel, A., Shao, M., Zeng, L. M., Wahner, A., Zhu,  
868 T., Zhang, Y. H., and Rohrer, F.: Missing OH source in a suburban environment near Beijing:  
869 observed and modelled OH and HO<sub>2</sub> concentrations in summer 2006, *Atmospheric Chemistry  
870 and Physics (ACP) & Discussions (ACPD)*, 2013.

871 Lu, X., Chen, N., Wang, Y., Cao, W., Zhu, B., Yao, T., Fung, J. C. H., and Lau, A. K. H.:  
872 Radical budget and ozone chemistry during autumn in the atmosphere of an urban site in  
873 central China, *Journal of Geophysical Research: Atmospheres*, 122, 3672-3685,  
874 <https://doi.org/10.1002/2016JD025676>, 2017.

875 Lyu, X., Wang, N., Guo, H., Xue, L., Jiang, F., Zeren, Y., Cheng, H., Cai, Z., Han, L., and  
876 Zhou, Y.: Causes of a continuous summertime O<sub>3</sub> pollution event in Jinan, a central city in the  
877 North China Plain, *Atmos. Chem. Phys.*, 19, 3025-3042, 10.5194/acp-19-3025-2019, 2019.

878 Lyu, X. P., Zeng, L. W., Guo, H., Simpson, I. J., Ling, Z. H., Wang, Y., Murray, F., Louie, P.  
879 K. K., Saunders, S. M., Lam, S. H. M., and Blake, D. R.: Evaluation of the effectiveness of air  
880 pollution control measures in Hong Kong, *Environmental Pollution*, 220, 87-94,  
881 <https://doi.org/10.1016/j.envpol.2016.09.025>, 2017.

882 Mazzuca, G. M., Ren, X., Loughner, C. P., Estes, M., Crawford, J. H., Pickering, K. E.,  
883 Weinheimer, A. J., and Dickerson, R. R.: Ozone production and its sensitivity to NO<sub>x</sub> and  
884 VOCs: results from the DISCOVER-AQ field experiment, Houston 2013, *Atmos. Chem.  
885 Phys.*, 13, 14463-14474, 2016.

886 McDuffie, E. E., Fibiger, D. L., Dubé, W. P., Lopez-Hilfiker, F., Lee, B. H., Thornton, J. A.,  
887 Shah, V., Jaeglé, L., Guo, H., Weber, R. J., Michael Reeves, J., Weinheimer, A. J., Schroder, J.  
888 C., Campuzano-Jost, P., Jimenez, J. L., Dibb, J. E., Veres, P., Ebben, C., Sparks, T. L.,  
889 Wooldridge, P. J., Cohen, R. C., Hornbrook, R. S., Apel, E. C., Campos, T., Hall, S. R.,  
890 Ullmann, K., and Brown, S. S.: Heterogeneous N<sub>2</sub>O<sub>5</sub> Uptake During Winter: Aircraft  
891 Measurements During the 2015 WINTER Campaign and Critical Evaluation of Current

892 Parameterizations, *Journal of Geophysical Research: Atmospheres*, 123, 4345-4372,  
893 10.1002/2018jd028336, 2018a.

894 McDuffie, E. E., Fibiger, D. L., Dubé, W. P., Lopez Hilfiker, F., Lee, B. H., Jaeglé, L., Guo,  
895 H., Weber, R. J., Reeves, J. M., Weinheimer, A. J., Schroder, J. C., Campuzano-Jost, P.,  
896 Jimenez, J. L., Dibb, J. E., Veres, P., Ebben, C., Sparks, T. L., Wooldridge, P. J., Cohen, R. C.,  
897 Campos, T., Hall, S. R., Ullmann, K., Roberts, J. M., Thornton, J. A., and Brown, S. S.:  
898 ClNO<sub>2</sub> Yields From Aircraft Measurements During the 2015 WINTER Campaign and Critical  
899 Evaluation of the Current Parameterization, *Journal of Geophysical Research: Atmospheres*,  
900 123, 12,994-913,015, <https://doi.org/10.1029/2018JD029358>, 2018b.

901 McDuffie, E. E., Womack, C. C., Fibiger, D. L., Dube, W. P., Franchin, A., Middlebrook, A.  
902 M., Goldberger, L., Lee, B. H., Thornton, J. A., Moravek, A., Murphy, J. G., Baasandorj, M.,  
903 and Brown, S. S.: On the contribution of nocturnal heterogeneous reactive nitrogen chemistry  
904 to particulate matter formation during wintertime pollution events in Northern Utah, *Atmos.*  
905 *Chem. Phys.*, 19, 9287-9308, 10.5194/acp-19-9287-2019, 2019.

906 Mozurkewich, M.: The dissociation constant of ammonium nitrate and its dependence on  
907 temperature, relative humidity and particle size, *Atmospheric Environment. Part A. General*  
908 *Topics*, 27, 261-270, [https://doi.org/10.1016/0960-1686\(93\)90356-4](https://doi.org/10.1016/0960-1686(93)90356-4), 1993.

909 Nenes, A., Pandis, S. N., Weber, R. J., and Russell, A.: Aerosol pH and liquid water content  
910 determine when particulate matter is sensitive to ammonia and nitrate availability, *Atmos.*  
911 *Chem. Phys.*, 20, 3249-3258, 10.5194/acp-20-3249-2020, 2020.

912 Novak, G. A., and Bertram, T. H.: Reactive VOC Production from Photochemical and  
913 Heterogeneous Reactions Occurring at the Air–Ocean Interface, *Accounts of Chemical*  
914 *Research*, 53, 1014-1023, 10.1021/acs.accounts.0c00095, 2020.

915 Pathak, R. K., Wu, W. S., and Wang, T.: Summertime PM<sub>2.5</sub> ionic species in  
916 four major cities of China: nitrate formation in an ammonia-deficient atmosphere, *Atmos.*  
917 *Chem. Phys.*, 9, 1711-1722, 10.5194/acp-9-1711-2009, 2009.

918 Pathak, R. K., Wang, T., and Wu, W. S.: Nighttime enhancement of PM<sub>2.5</sub> nitrate in  
919 ammonia-poor atmospheric conditions in Beijing and Shanghai: Plausible contributions of  
920 heterogeneous hydrolysis of N<sub>2</sub>O<sub>5</sub> and HNO<sub>3</sub> partitioning, *Atmospheric Environment*, 45,  
921 1183-1191, <https://doi.org/10.1016/j.atmosenv.2010.09.003>, 2011.

922 Prabhakar, G., Parworth, C. L., Zhang, X., Kim, H., Young, D. E., Beyersdorf, A. J., Ziemba,  
923 L. D., Nowak, J. B., Bertram, T. H., Faloona, I. C., Zhang, Q., and Cappa, C. D.:  
924 Observational assessment of the role of nocturnal residual-layer chemistry in determining  
925 daytime surface particulate nitrate concentrations, *Atmos. Chem. Phys.*, 17, 14747-14770,  
926 10.5194/acp-17-14747-2017, 2017.

927 Qin, Y. M., Tan, H. B., Li, Y. J., Schurman, M. I., Li, F., Canonaco, F., Prévôt, A. S. H., and  
928 Chan, C. K.: Impacts of traffic emissions on atmospheric particulate nitrate and organics at a

929 downwind site on the periphery of Guangzhou, China, *Atmos. Chem. Phys.*, 17, 10245-  
930 10258, 10.5194/acp-17-10245-2017, 2017.

931 Riedel, T. P., Wolfe, G. M., Danas, K. T., Gilman, J. B., Kuster, W. C., Bon, D. M., Vlasenko,  
932 A., Li, S. M., Williams, E. J., Lerner, B. M., Veres, P. R., Roberts, J. M., Holloway, J. S.,  
933 Lefer, B., Brown, S. S., and Thornton, J. A.: An MCM modeling study of nitryl chloride  
934 (CINO<sub>2</sub>) impacts on oxidation, ozone production and nitrogen oxide partitioning  
935 in polluted continental outflow, *Atmos. Chem. Phys.*, 14, 3789-3800, 10.5194/acp-14-3789-  
936 2014, 2014.

937 Romer, P. S., Wooldridge, P. J., Crouse, J. D., Kim, M. J., Wennberg, P. O., Dibb, J. E.,  
938 Scheuer, E., Blake, D. R., Meinardi, S., Brosius, A. L., Thames, A. B., Miller, D. O., Brune,  
939 W. H., Hall, S. R., Ryerson, T. B., and Cohen, R. C.: Constraints on Aerosol Nitrate  
940 Photolysis as a Potential Source of HONO and NO<sub>x</sub>, *Environmental Science & Technology*,  
941 52, 13738-13746, 10.1021/acs.est.8b03861, 2018.

942 Saunders, S. M., Jenkin, M. E., Derwent, R. G., and Pilling, M. J.: Protocol for the  
943 development of the Master Chemical Mechanism, MCM v3 (Part A): tropospheric  
944 degradation of non-aromatic volatile organic compounds, *Atmos. Chem. Phys.*, 3, 161-180,  
945 10.5194/acp-3-161-2003, 2003.

946 Stelson, A. W., and Seinfeld, J. H.: Relative humidity and temperature dependence of the  
947 ammonium nitrate dissociation constant, *Atmospheric Environment* (1967), 16, 983-992,  
948 [https://doi.org/10.1016/0004-6981\(82\)90184-6](https://doi.org/10.1016/0004-6981(82)90184-6), 1982.

949 Su, T., Li, J., Tian, C., Zong, Z., Chen, D., and Zhang, G.: Source and formation of fine  
950 particulate nitrate in South China: Constrained by isotopic modeling and online trace gas  
951 analysis, *Atmospheric Environment*, 231, 117563,  
952 <https://doi.org/10.1016/j.atmosenv.2020.117563>, 2020.

953 Tan, Z., Lu, K., Jiang, M., Su, R., Dong, H., Zeng, L., Xie, S., Tan, Q., and Zhang, Y.:  
954 Exploring ozone pollution in Chengdu, southwestern China: A case study from radical  
955 chemistry to O<sub>3</sub>-VOC-NO<sub>x</sub> sensitivity, *Science of The Total Environment*, 636, 775-786,  
956 <https://doi.org/10.1016/j.scitotenv.2018.04.286>, 2018.

957 Tang, G., Wang, Y., Liu, Y., Wu, S., Huang, X., Yang, Y., Wang, Y., Ma, J., Bao, X., Liu, Z., Ji,  
958 D., Li, T., Li, X., and Wang, Y.: Low particulate nitrate in the residual layer in autumn over  
959 the North China Plain, *Science of The Total Environment*, 782, 146845,  
960 <https://doi.org/10.1016/j.scitotenv.2021.146845>, 2021.

961 Tao, J., Zhang, Z., Tan, H., Zhang, L., Wu, Y., Sun, J., Che, H., Cao, J., Cheng, P., Chen, L.,  
962 and Zhang, R.: Observational evidence of cloud processes contributing to daytime elevated  
963 nitrate in an urban atmosphere, *Atmospheric Environment*, 186, 209-215,  
964 <https://doi.org/10.1016/j.atmosenv.2018.05.040>, 2018.

965 Tao, Y., Ye, X., Ma, Z., Xie, Y., Wang, R., Chen, J., Yang, X., and Jiang, S.: Insights into

966 different nitrate formation mechanisms from seasonal variations of secondary inorganic  
967 aerosols in Shanghai, *Atmospheric Environment*, 145, 1-9,  
968 <https://doi.org/10.1016/j.atmosenv.2016.09.012>, 2016.

969 von Bobruzki, K., Braban, C. F., Famulari, D., Jones, S. K., Blackall, T., Smith, T. E. L.,  
970 Blom, M., Coe, H., Gallagher, M., Ghalaieny, M., McGillen, M. R., Percival, C. J.,  
971 Whitehead, J. D., Ellis, R., Murphy, J., Mohacsi, A., Pogany, A., Junninen, H., Rantanen, S.,  
972 Sutton, M. A., and Nemitz, E.: Field inter-comparison of eleven atmospheric ammonia  
973 measurement techniques, *Atmos. Meas. Tech.*, 3, 91-112, 10.5194/amt-3-91-2010, 2010.

974 Wang, C., Yuan, B., Wu, C., Wang, S., Qi, J., Wang, B., Wang, Z., Hu, W., Chen, W., Ye, C.,  
975 Wang, W., Sun, Y., Wang, C., Huang, S., Song, W., Wang, X., Yang, S., Zhang, S., Xu, W.,  
976 Ma, N., Zhang, Z., Jiang, B., Su, H., Cheng, Y., Wang, X., and Shao, M.: Measurements of  
977 higher alkanes using NO<sup>+</sup> chemical ionization in PTR-ToF-MS: important contributions of  
978 higher alkanes to secondary organic aerosols in China, *Atmos. Chem. Phys.*, 20, 14123-  
979 14138, 10.5194/acp-20-14123-2020, 2020a.

980 Wang, H., Lu, K., Chen, X., Zhu, Q., Chen, Q., Guo, S., Jiang, M., Li, X., Shang, D., Tan, Z.,  
981 Wu, Y., Wu, Z., Zou, Q., Zheng, Y., Zeng, L., Zhu, T., Hu, M., and Zhang, Y.: High N<sub>2</sub>O<sub>5</sub>  
982 Concentrations Observed in Urban Beijing: Implications of a Large Nitrate Formation  
983 Pathway, *Environmental Science & Technology Letters*, 4, 416-420,  
984 10.1021/acs.estlett.7b00341, 2017a.

985 Wang, H., Lu, K., Tan, Z., Sun, K., Li, X., Hu, M., Shao, M., Zeng, L., Zhu, T., and Zhang, Y.:  
986 Model simulation of NO<sub>3</sub>, N<sub>2</sub>O<sub>5</sub> and ClNO<sub>2</sub> at a rural site in Beijing during CAREBeijing-  
987 2006, *Atmospheric Research*, 196, 97-107, <https://doi.org/10.1016/j.atmosres.2017.06.013>,  
988 2017b.

989 Wang, H., Lu, K., Chen, X., Zhu, Q., Wu, Z., Wu, Y., and Sun, K.: Fast particulate nitrate  
990 formation via N<sub>2</sub>O<sub>5</sub> uptake aloft in winter in Beijing, *Atmos. Chem. Phys.*, 18, 10483-10495,  
991 10.5194/acp-18-10483-2018, 2018a.

992 Wang, H., Lu, K., Guo, S., Wu, Z., Shang, D., Tan, Z., Wang, Y., Le Breton, M., Lou, S.,  
993 Tang, M., Wu, Y., Zhu, W., Zheng, J., Zeng, L., Hallquist, M., Hu, M., and Zhang, Y.:  
994 Efficient N<sub>2</sub>O<sub>5</sub> uptake and NO<sub>3</sub> oxidation in the outflow of urban Beijing, *Atmos. Chem.*  
995 *Phys.*, 18, 9705-9721, 10.5194/acp-18-9705-2018, 2018b.

996 Wang, N., Guo, H., Jiang, F., Ling, Z. H., and Wang, T.: Simulation of ozone formation at  
997 different elevations in mountainous area of Hong Kong using WRF-CMAQ model, *Science of*  
998 *The Total Environment*, 505, 939-951, <https://doi.org/10.1016/j.scitotenv.2014.10.070>, 2015.

999 Wang, N., Lyu, X., Deng, X., Huang, X., Jiang, F., and Ding, A.: Aggravating O<sub>3</sub> pollution  
1000 due to NO<sub>x</sub> emission control in eastern China, *Science of The Total Environment*, 677, 732-  
1001 744, <https://doi.org/10.1016/j.scitotenv.2019.04.388>, 2019.

1002 Wang, Y., Zhang, Y., Hao, J., and Luo, M.: Seasonal and spatial variability of surface ozone

1003 over China: contributions from background and domestic pollution, *Atmos. Chem. Phys.*, 11,  
1004 3511-3525, 10.5194/acp-11-3511-2011, 2011.

1005 Wang, Z., Yuan, B., Ye, C., Roberts, J., Wisthaler, A., Lin, Y., Li, T., Wu, C., Peng, Y., Wang,  
1006 C., Wang, S., Yang, S., Wang, B., Qi, J., Wang, C., Song, W., Hu, W., Wang, X., Xu, W., Ma,  
1007 N., Kuang, Y., Tao, J., Zhang, Z., Su, H., Cheng, Y., Wang, X., and Shao, M.: High  
1008 Concentrations of Atmospheric Isocyanic Acid (HNCO) Produced from Secondary Sources in  
1009 China, *Environmental Science & Technology*, 54, 11818-11826, 10.1021/acs.est.0c02843,  
1010 2020b.

1011 Watson, J. G.: Visibility: Science and Regulation, *Journal of The Air & Waste Management*  
1012 Association, 52, 973-999, 2002.

1013 Wen, L., Chen, J., Yang, L., Wang, X., Caihong, X., Sui, X., Yao, L., Zhu, Y., Zhang, J., Zhu,  
1014 T., and Wang, W.: Enhanced formation of fine particulate nitrate at a rural site on the North  
1015 China Plain in summer: The important roles of ammonia and ozone, *Atmospheric*  
1016 *Environment*, 101, 294-302, <https://doi.org/10.1016/j.atmosenv.2014.11.037>, 2015.

1017 Wen, L., Xue, L., Wang, X., Xu, C., Chen, T., Yang, L., Wang, T., Zhang, Q., and Wang, W.:  
1018 Summertime fine particulate nitrate pollution in the North China Plain: increasing trends,  
1019 formation mechanisms and implications for control policy, *Atmos. Chem. Phys.*, 18, 11261-  
1020 11275, 10.5194/acp-18-11261-2018, 2018.

1021 Wolfe, G. M., Marvin, M. R., Roberts, S. J., Travis, K. R., and Liao, J.: The Framework for 0-  
1022 D Atmospheric Modeling (F0AM) v3.1, *Geosci. Model Dev.*, 9, 3309-3319, 10.5194/gmd-9-  
1023 3309-2016, 2016.

1024 Womack, C. C., McDuffie, E. E., Edwards, P. M., Bares, R., de Gouw, J. A., Docherty, K. S.,  
1025 Dube, W. P., Fibiger, D. L., Franchin, A., Gilman, J. B., Goldberger, L., Lee, B. H., Lin, J. C.,  
1026 Long, R., Middlebrook, A. M., Millet, D. B., Moravek, A., Murphy, J. G., Quinn, P. K.,  
1027 Riedel, T. P., Roberts, J. M., Thornton, J. A., Valin, L. C., Veres, P. R., Whitehill, A. R., Wild,  
1028 R. J., Warneke, C., Yuan, B., Baasandorj, M., and Brown, S. S.: An odd oxygen framework  
1029 for wintertime ammonium nitrate aerosol pollution in urban areas: NO<sub>x</sub> and VOC control as  
1030 mitigation strategies, *Geophysical Research Letters*, 0, 10.1029/2019gl082028, 2019.

1031 Wu, C., Wang, C., Wang, S., Wang, W., Yuan, B., Qi, J., Wang, B., Wang, H., Wang, C., Song,  
1032 W., Wang, X., Hu, W., Lou, S., Ye, C., Peng, Y., Wang, Z., Huangfu, Y., Xie, Y., Zhu, M.,  
1033 Zheng, J., Wang, X., Jiang, B., Zhang, Z., and Shao, M.: Measurement report: Important  
1034 contributions of oxygenated compounds to emissions and chemistry of volatile organic  
1035 compounds in urban air, *Atmos. Chem. Phys.*, 20, 14769-14785, 10.5194/acp-20-14769-2020,  
1036 2020.

1037 Xu, L., and Penner, J. E.: Global simulations of nitrate and ammonium aerosols and their  
1038 radiative effects, *Atmos. Chem. Phys.*, 12, 9479-9504, 10.5194/acp-12-9479-2012, 2012.

1039 Xue, J., Yuan, Z., Lau, A. K. H., and Yu, J. Z.: Insights into factors affecting nitrate in PM<sub>2.5</sub>

1040 in a polluted high NO<sub>x</sub> environment through hourly observations and size distribution  
1041 measurements, *Journal of Geophysical Research: Atmospheres*, 119, 4888-4902,  
1042 10.1002/2013JD021108, 2014a.

1043 Xue, L. K., Wang, T., Gao, J., Ding, A. J., Zhou, X. H., Blake, D. R., Wang, X. F., Saunders,  
1044 S. M., Fan, S. J., Zuo, H. C., Zhang, Q. Z., and Wang, W. X.: Ground-level ozone in four  
1045 Chinese cities: precursors, regional transport and heterogeneous processes, *Atmos. Chem.*  
1046 *Phys.*, 14, 13175-13188, 10.5194/acp-14-13175-2014, 2014b.

1047 Yang, Q., Su, H., Li, X., Cheng, Y., Lu, K., Cheng, P., Gu, J., Guo, S., Hu, M., and Zeng, L.:  
1048 Daytime HONO formation in the suburban area of the megacity Beijing, China, *Science*  
1049 *China Chemistry*, 57, 1032-1042, 2014.

1050 Yang, T., Sun, Y., Zhang, W., Wang, Z., Liu, X., Fu, P., and Wang, X.: Evolutionary processes  
1051 and sources of high-nitrate haze episodes over Beijing, Spring, *Journal of Environmental*  
1052 *Sciences*, 54, 142-151, <https://doi.org/10.1016/j.jes.2016.04.024>, 2017.

1053 Ye, C., Gao, H., Zhang, N., and Zhou, X.: Photolysis of Nitric Acid and Nitrate on Natural  
1054 and Artificial Surfaces, *Environmental Science & Technology*, 50, 3530-3536,  
1055 10.1021/acs.est.5b05032, 2016.

1056 Ye, C., Zhang, N., Gao, H., and Zhou, X.: Photolysis of Particulate Nitrate as a Source of  
1057 HONO and NO<sub>x</sub>, *Environmental Science & Technology*, 51, 6849-6856,  
1058 10.1021/acs.est.7b00387, 2017.

1059 Ye, C., Yuan, B., Lin, Y., Wang, Z., Hu, W., Li, T., Chen, W., Wu, C., Wang, C., Huang, S., Qi,  
1060 J., Wang, B., Wang, C., Song, W., Wang, X., Zheng, E., Krechmer, J. E., Ye, P., Zhang, Z.,  
1061 Wang, X., Worsnop, D. R., and Shao, M.: Chemical characterization of oxygenated organic  
1062 compounds in the gas phase and particle phase using iodide CIMS with FIGAERO in urban  
1063 air, *Atmospheric Chemistry and Physics*, 21, 8455-8478, 10.5194/acp-21-8455-2021, 2021.

1064 Yu, C., Wang, Z., Xia, M., Fu, X., Wang, W., Tham, Y. J., Chen, T., Zheng, P., Li, H., Shan, Y.,  
1065 Wang, X., Xue, L., Zhou, Y., Yue, D., Ou, Y., Gao, J., Lu, K., Brown, S. S., Zhang, Y., and  
1066 Wang, T.: Heterogeneous N<sub>2</sub>O<sub>5</sub> reactions on atmospheric aerosols at four Chinese sites:  
1067 improving model representation of uptake parameters, *Atmos. Chem. Phys.*, 20, 4367-4378,  
1068 10.5194/acp-20-4367-2020, 2020.

1069 Yu, Y., Cheng, P., Li, H., Yang, W., Han, B., Song, W., Hu, W., Wang, X., Yuan, B., Shao, M.,  
1070 Huang, Z., Li, Z., Zheng, J., Wang, H., and Yu, X.: Budget of nitrous acid (HONO) and its  
1071 impacts on atmospheric oxidation capacity at an urban site in the fall season of Guangzhou,  
1072 China, *Atmos. Chem. Phys. Discuss.*, 2021, 1-38, 10.5194/acp-2021-178, 2021.

1073 Yuan, B., Chen, W., Shao, M., Wang, M., Lu, S., Wang, B., Liu, Y., Chang, C., and Wang, B.:  
1074 Measurements of ambient hydrocarbons and carbonyls in the Pearl River Delta (PRD), China,  
1075 *Atmospheric Research*, 116, 93-104, 2012.

1076 Yuan, B., Liggió, J., Wentzell, J., Li, S. M., Stark, H., Roberts, J. M., Gilman, J., Lerner, B.,



1077 Warneke, C., Li, R., Leithead, A., Osthoff, H. D., Wild, R., Brown, S. S., and de Gouw, J. A.:  
 1078 Secondary formation of nitrated phenols: insights from observations during the Uintah Basin  
 1079 Winter Ozone Study (UBWOS) 2014, *Atmos. Chem. Phys.*, 16, 2139-2153, 10.5194/acp-16-  
 1080 2139-2016, 2016.

1081 Yun, H., Wang, T., Wang, W., Tham, Y. J., Li, Q., Wang, Z., and Poon, S. C. N.: Nighttime  
 1082 NO<sub>x</sub> loss and ClNO<sub>2</sub> formation in the residual layer of a polluted region: Insights from field  
 1083 measurements and an iterative box model, *Science of The Total Environment*, 622-623, 727-  
 1084 734, <https://doi.org/10.1016/j.scitotenv.2017.11.352>, 2018a.

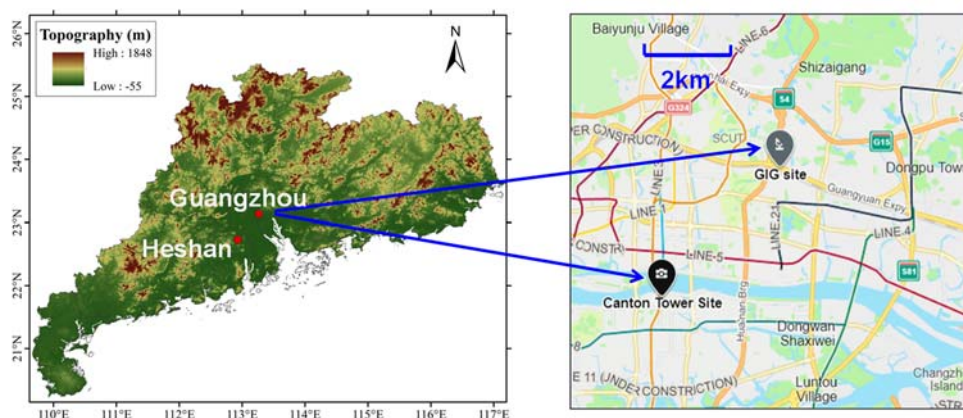
1085 Yun, H., Wang, W., Wang, T., Xia, M., Yu, C., Wang, Z., Poon, S. C. N., Yue, D., and Zhou,  
 1086 Y.: Nitrate formation from heterogeneous uptake of dinitrogen pentoxide during a severe  
 1087 winter haze in southern China, *Atmos. Chem. Phys.*, 18, 17515-17527, 10.5194/acp-18-  
 1088 17515-2018, 2018b.

1089 Zhai, S., Jacob, D. J., Wang, X., Liu, Z., Wen, T., Shah, V., Li, K., Moch, J. M., Bates, K. H.,  
 1090 Song, S., Shen, L., Zhang, Y., Luo, G., Yu, F., Sun, Y., Wang, L., Qi, M., Tao, J., Gui, K., Xu,  
 1091 H., Zhang, Q., Zhao, T., Wang, Y., Lee, H. C., Choi, H., and Liao, H.: Control of particulate  
 1092 nitrate air pollution in China, *Nature Geoscience*, 10.1038/s41561-021-00726-z, 2021.

1093 Zhang, H., An, Q., Zhao, S., Xie, B., and Liu, Q.: Advances in the research of optical  
 1094 properties and radiative forcing of nitrate aerosols, *Acta Meteorologica Sinica*, 75, 539-551,  
 1095 2017.

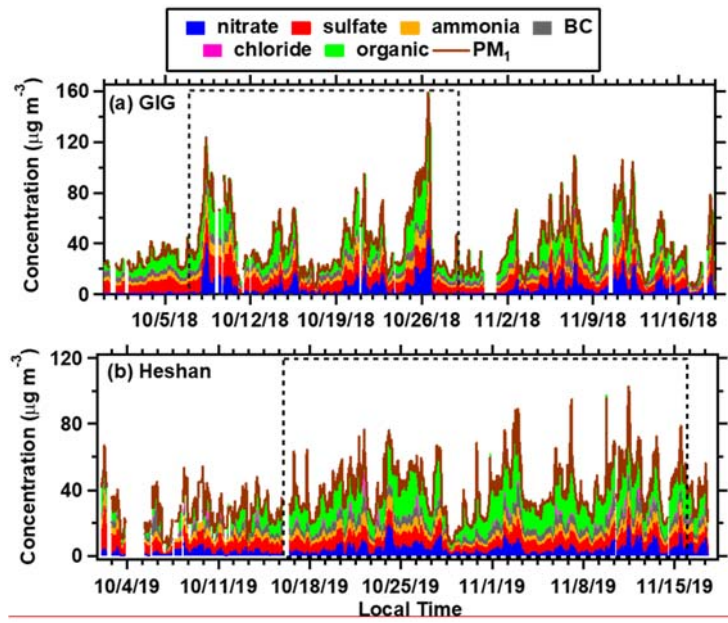
1096 Zhang, R., Gen, M., Huang, D., Li, Y., and Chan, C. K.: Enhanced Sulfate Production by  
 1097 Nitrate Photolysis in the Presence of Halide Ions in Atmospheric Particles, *Environmental  
 1098 Science & Technology*, 54, 3831-3839, 10.1021/acs.est.9b06445, 2020.

1099 Zhou, S., Wu, L., Guo, J., Chen, W., Wang, X., Zhao, J., Cheng, Y., Huang, Z., Zhang, J., Sun,  
 1100 Y., Fu, P., Jia, S., Tao, J., Chen, Y., and Kuang, J.: Measurement report: Vertical distribution  
 1101 of atmospheric particulate matter within the urban boundary layer in southern China – size-  
 1102 segregated chemical composition and secondary formation through cloud processing and  
 1103 heterogeneous reactions, *Atmos. Chem. Phys.*, 20, 6435-6453, 10.5194/acp-20-6435-2020,  
 1104 2020.

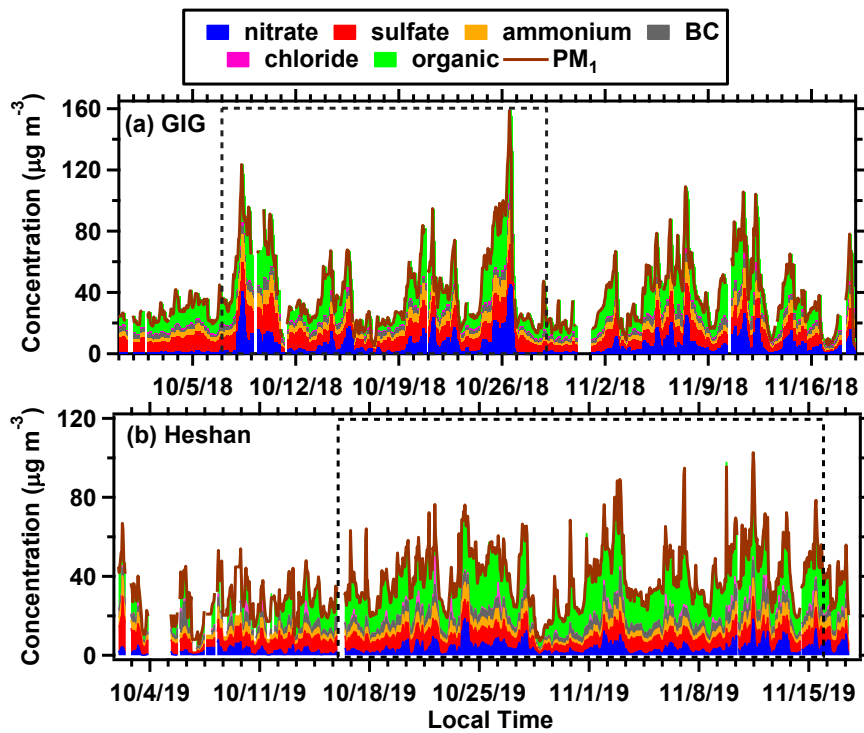


1105

1106 **Figure 1.** Sampling site at Guangzhou Institute of Geochemistry, Chinese Academy of  
1107 Sciences (GIG), Heshan and Canton Tower. Note that the map is extracted from  
1108 Microsoft Bing maps by the authors.  
1109

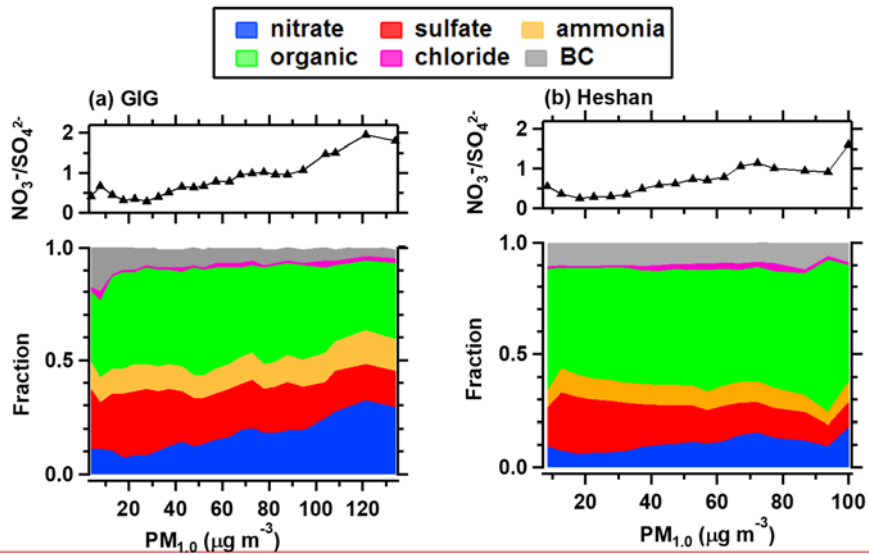


1110

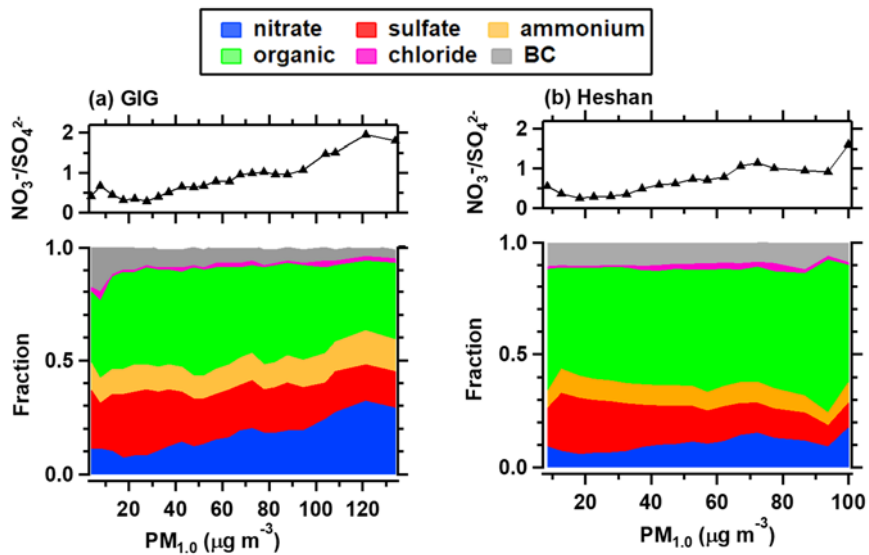


1111

1112 **Figure 2.** Temporal variations of the mass concentration of the major chemical  
 1113 components in  $PM_{10}$  including nitrate ( $NO_3^-$ ), sulfate ( $SO_4^{2-}$ ), ammonium ( $NH_4^+$ ), black  
 1114 carbon (BC), chloride ( $Cl^-$ ) and organics at (a) GIG site and (b) Heshan site. The black  
 1115 dashed rectangle represents the investigated period which had complete set of data.  
 1116



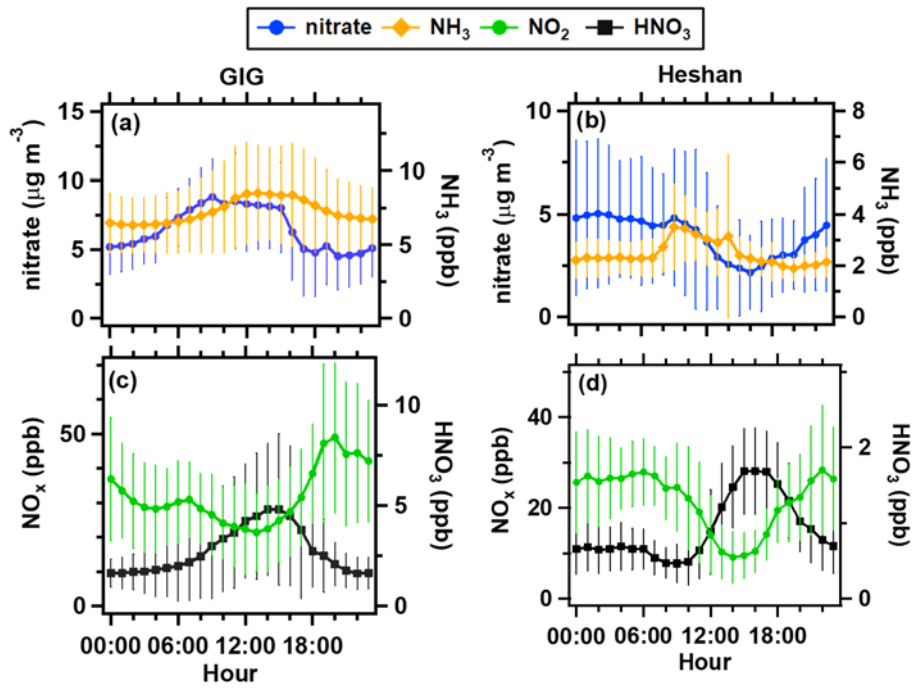
1117



1118

1119 **Figure 3.** The mass concentration ratio of  $NO_3^-/SO_4^{2-}$  (top) and fractions of major  
 1120 chemical components (bottom) in  $PM_{1.0}$  at (a) GIG site and (b) Heshan site.

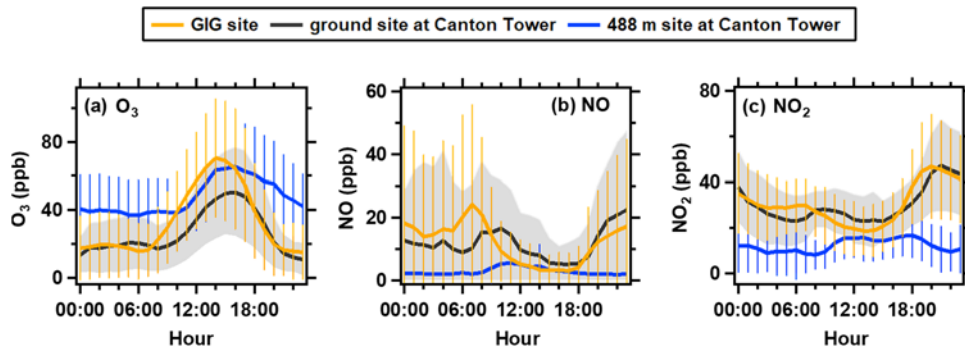
1121



1122

1123 **Figure 4.** Diurnal variations of mean concentrations of nitrate and related pollution  
 1124 species at (a) GIG site and (b) Heshan site. The error bars represent the standard  
 1125 deviation of the means.

1126

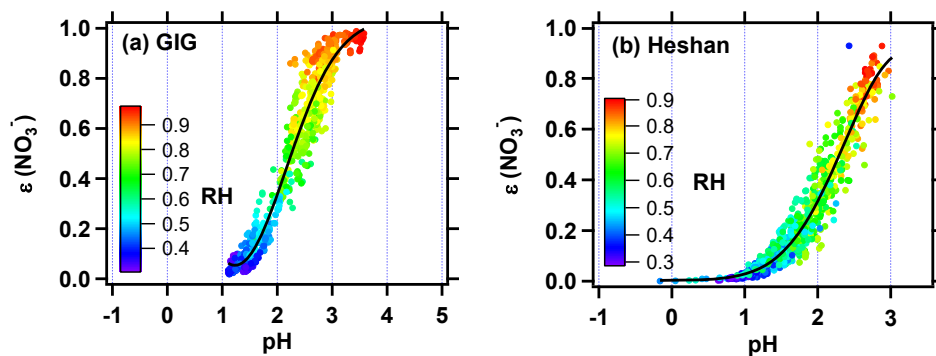


1128

1129 **Figure 5.** Diurnal variation of mean concentrations of (a) O<sub>3</sub>, (b) NO, (c) NO<sub>2</sub> at GIG  
 1130 (orange lines), and the ground and 488m sites of Canton Tower (black and blue lines,  
 1131 respectively). The orange and blue error bars represent the standard deviations of the  
 1132 mean concentrations at the GIG site and the 488m site of Canton Tower, the grey areas  
 1133 show one standard deviation of the mean concentration at ground site of Canton Tower.

1134

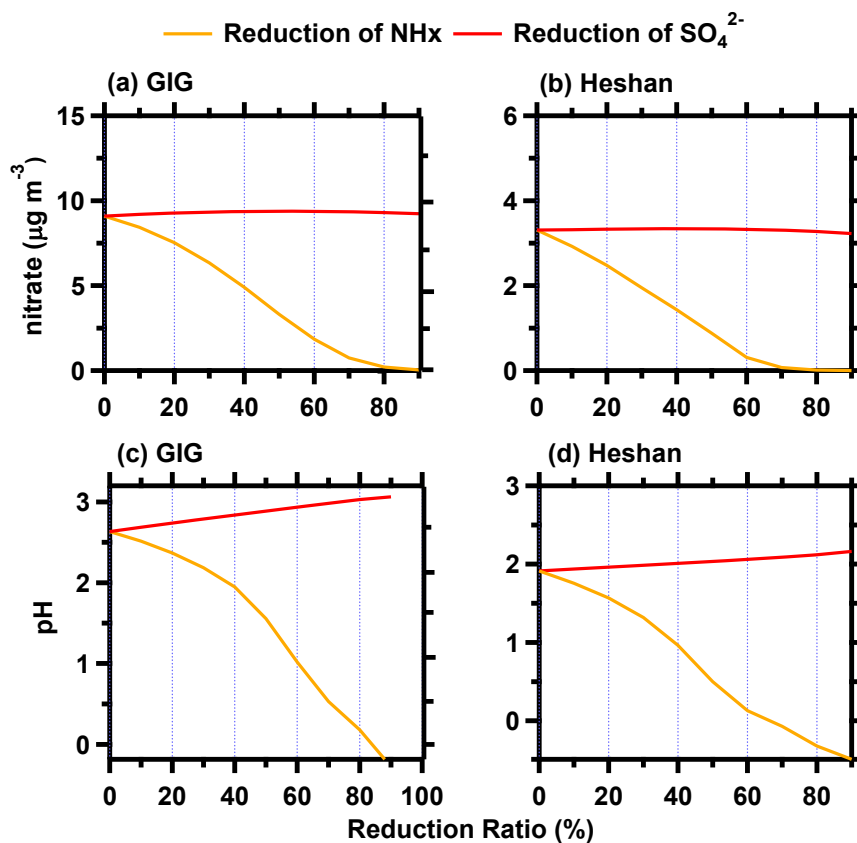
1135



1136

1137 **Figure 6.** The particle fraction of nitrate in the sum of  $\text{HNO}_3$ +nitrate ( $\epsilon(\text{NO}_3^-)$ ) against  
 1138 aerosol pH. The pH data are colored by relative humidity and fit to an “s-curve” in  
 1139 black line, as shown in Guo et al. (2018).

1140



1141

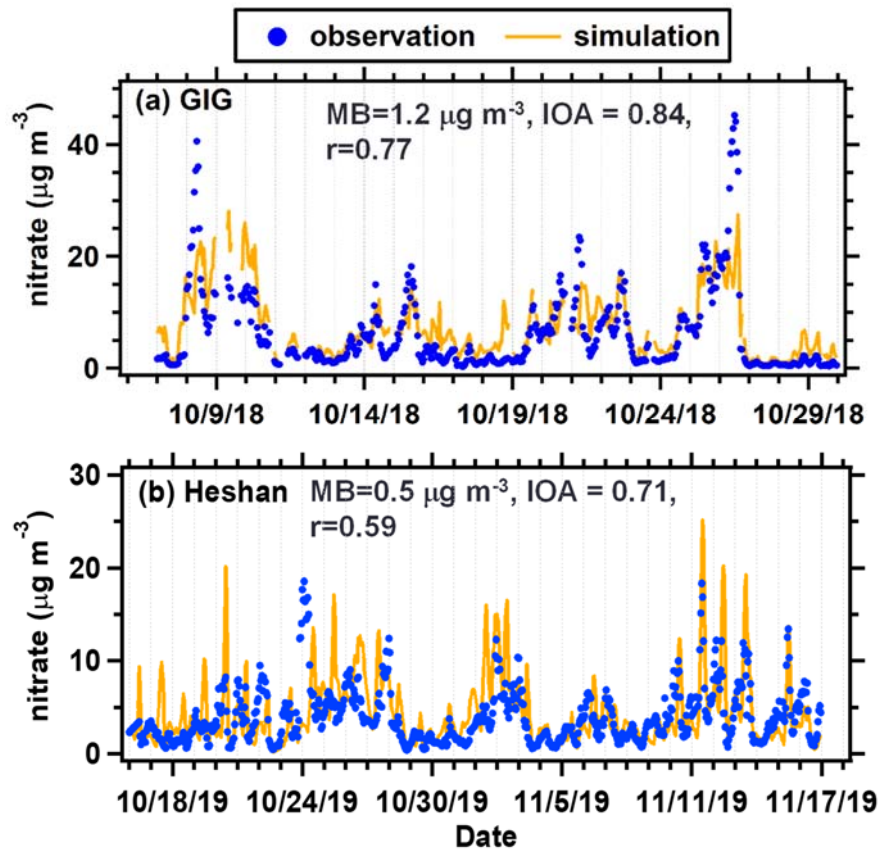
1142 **Figure 7.** ISORROPIA-predicted average nitrate (a, b) and pH (c, d) as a function of

1143 changes in  $\text{NH}_x$  (ammonium +  $\text{NH}_3$ , orange line) and  $\text{SO}_4^{2-}$  (red line) at the GIG and

1144 Heshan site during the study period.

1145

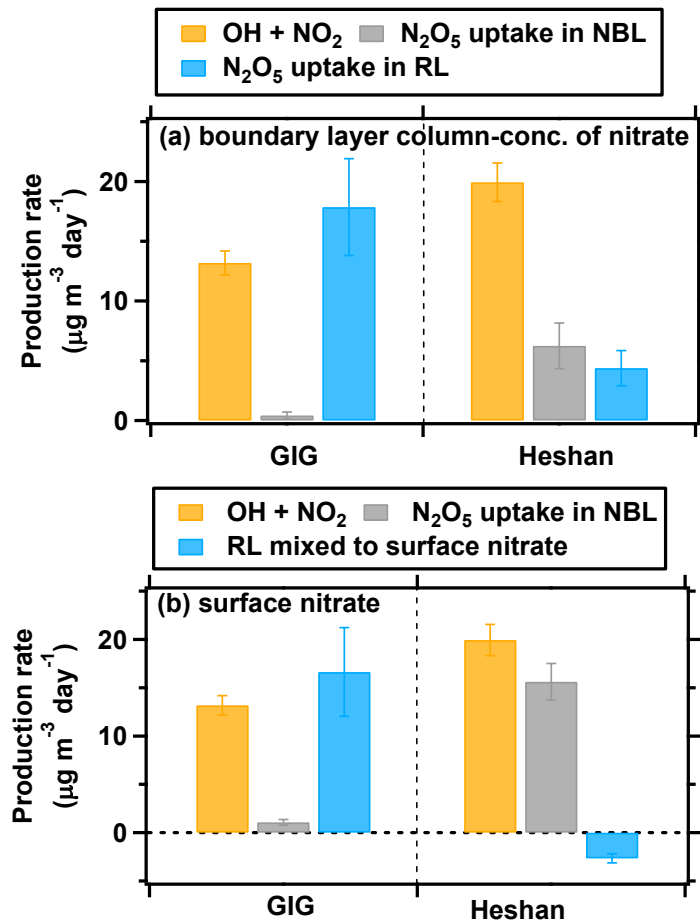




1147

1148 **Figure 86.** Comparison of the temporal box model simulated and observed nitrate at  
 1149 the (a) GIG site and (b) Heshan site.

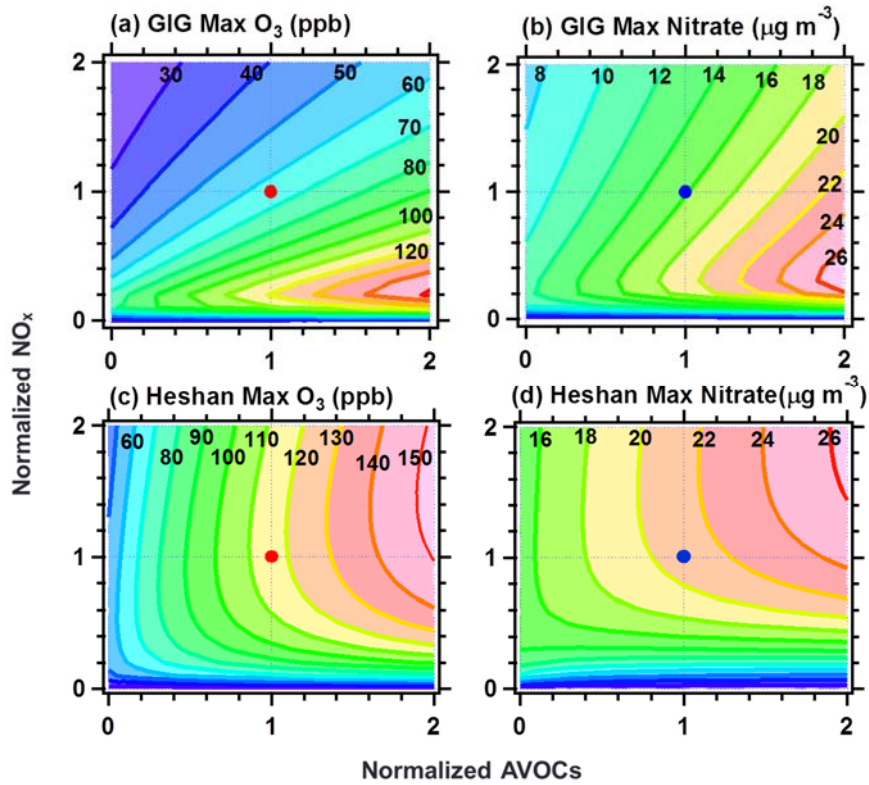
1150



1151

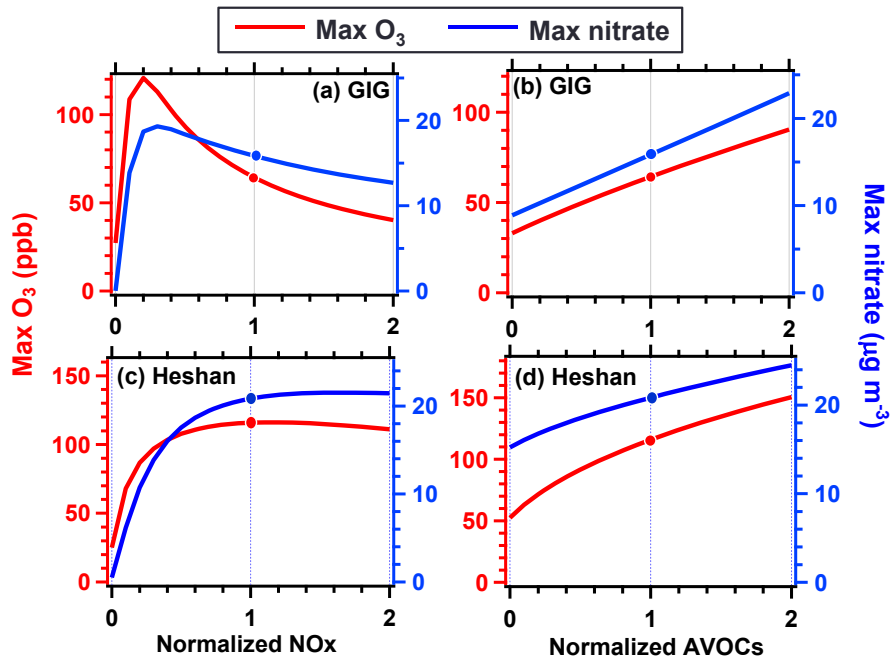
1152 **Figure 97.** The daily-averaged contribution (a) to boundary layer column concentration  
 1153 and (b) to surface nitrate from three pathways (OH +NO<sub>2</sub> reaction, N<sub>2</sub>O<sub>5</sub> uptake in NBL,  
 1154 and N<sub>2</sub>O<sub>5</sub> uptake in RL/N<sub>2</sub>O<sub>5</sub> uptake from RL mixed process) at the GIG and Heshan  
 1155 sites. The error bars represent the standard deviations of the mean production rate.

1156



1158

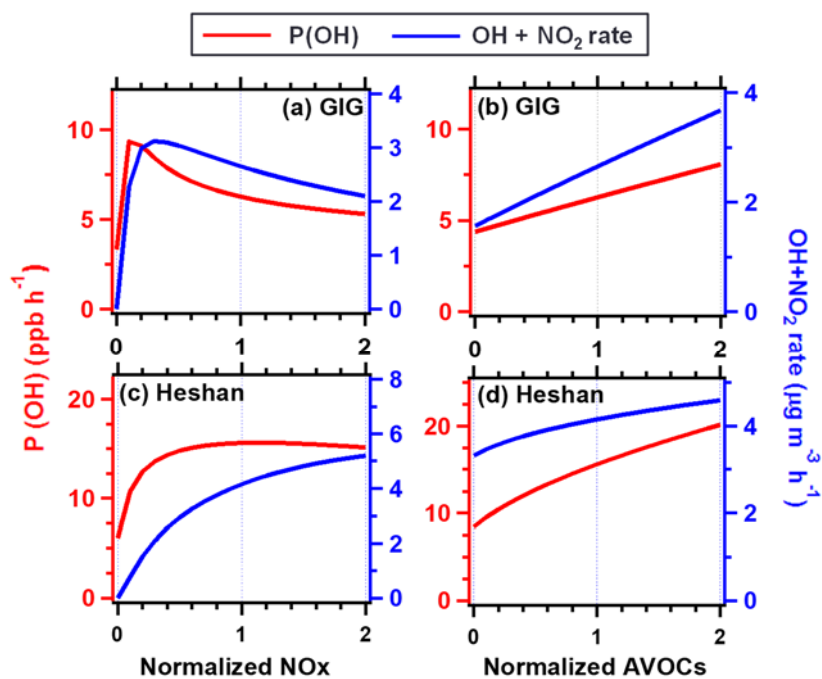
1159 **Figure 108.** The simulated isopleths of ozone and nitrate with normalized NO<sub>x</sub> and  
 1160 AVOCs concentration at the (a, b) GIG site and (c, d) Heshan site, each isopleth  
 1161 represents the maximum ozone and nitrate in the simulation, and the red and blue circles  
 1162 represent the base cases.  
 1163



1164

1165 **Figure 119.** Simulated maximum ozone and nitrate concentration with normalized  
 1166 NO<sub>x</sub> and AVOCs at the (a, b) GIG site and (c, d) Heshan site, cutting through the  
 1167 simulated isopleth in Figure 8 with normalized AVOCs and NO<sub>x</sub> ratio at 1, respectively.  
 1168 The red and blue circles represent the base cases.

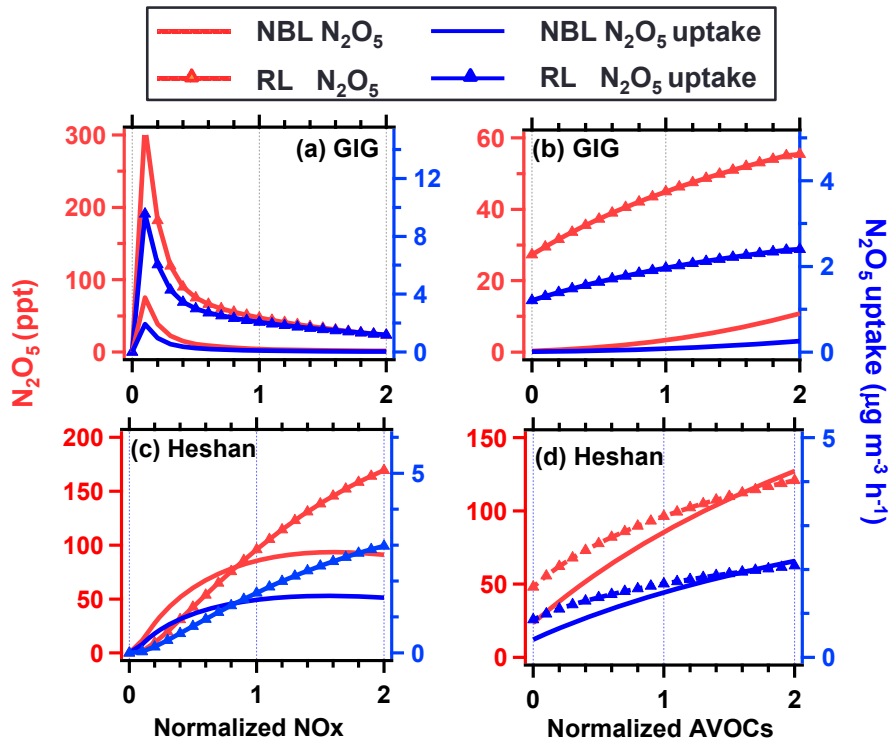
1169



1170

1171 **Figure 120.** Simulated average production rates of OH (P (OH)) and the reaction rate  
 1172 of OH and NO<sub>2</sub> with the normalized changes of NO<sub>x</sub> and AVOCs emissions at the (a,  
 1173 b) GIG site and (c, d) Heshan site.

1174



1175

1176 **Figure 131.** Simulated average concentration of  $N_2O_5$  and nitrate production rate of  
 1177 from  $N_2O_5$  uptake with the normalized changes of  $NO_x$  and AVOCs emissions at the (a,  
 1178 b) GIG site and (c, d) Heshan site in the NBL and RL.

1179